Global Satellite Observations for Smart Cities

Zhong Liu[1, 2], Menglin S. Jin[3], Jacqueline Liu[4], Angela Li[1], William Teng[1, 5], Bruce Vollmer[1], and D. Meyer[1]

[1]NASA Goddard Earth Sciences Data and Information Services Center, Godard Space Flight Center, Greenbelt, Maryland, USA

[2]Center for Spatial Information Science and Systems, George Mason University, Virginia, USA

[3]Department of Atmospheric and Oceanic Science, University of Maryland at College Park, Maryland, USA

[4]Urbana High School, Urbana, Maryland, USA

[5]Adnet Systems Inc., Greenbelt, Maryland, USA

Submitted to:

"Data Analytics Applications for Smart Cities"

Editors: Dr. Amir H. Alavi and Dr. William G. Buttlar

Auerbach/CRC Press, Taylor & Francis Group

September 15, 2017 (submitted)

January 24, 2018 (revised)

1. **Introduction**

Over the past several decades, the number of megacities (exceeding 10 million people in population) has been rapidly growing around the world as a result of rapid economic growth and unprecedented urbanization (United Nations 2014). For example, in Asia alone, more than 30 cities (Fig. 1) are listed as megacities (e.g., Tokyo, Shanghai, Guangzhou), demanding effective management for city planning, operations, and disaster mitigation. The smart city approach requires data and information to be collected from multiple sources and to be integrated with modern technologies, providing a new and cost-effective way for decision makers to manage cities in different sizes around the world as well as making information publicly available for city residents.

Environmental information at different spatial and temporal scales (e.g., ranging from local to regional and from real time to climate) is one of critical sources for city planning, management, and disaster mitigation (Seto 2011). Each year, severe weather events (e.g., heavy rain or snowfall, tropical cyclones, heat waves) can strike a city around the world without warning and cause severe damage to a city's infrastructure as well as interrupt people's daily life. Effective management of water, air pollution, energy, etc. requires environmental data to be available at anytime and on demand. Nonetheless, making data available for timely and easy access is critically important for effective city planning and management activities (Seto 2011).

Climate change can have a profound impact on cities around the world. For example, for cities in tropical and sub-tropical regions, changes in heavy rainfall amount as well as tropical cyclone size, frequency, and intensity can impact a city's operations, infrastructure, development, and long-term planning. Sea level rise is another major concern for city managers and residents in coastal cities. To be able to monitor and predict such change is critical for a

47 city's planning and operations and all cannot be done without environmental data.

48 On the other hand, studies show that cities, especially large cities, can have an impact on
49 local weather (e.g., Zhang et al. 2017; Jin et al. 2005, 2010, 2011; Shepherd and Jin 2004; Seto
50 and Shepherd 2009; Kauffmann et al. 2007; Guo et al. 2016). Activities from urbanization and
51 city development can dramatically modify its surrounding natural environment and landscape.
52 For example, urban heat islands (UHI) provide manmade heat sources that can change its
53 surrounding atmospheric environment and potentially fuel severe weather. Air pollution that is
54 associated with automobiles, industries, etc. supplies the atmosphere with aerosols that could
55 modify meteorological processes such as clouds and precipitation (Jin et al. 2005, 2011).

56 Nonetheless, the few examples above have shown the importance of environmental data
57 in city's planning and management. Such data consist of multi-disciplines at multi-scales in
58 space and time. Traditional ground-based observations (e.g. rain gauges, automatic weather
59 stations) have limitations because it is costly and time-consuming to deploy such measurements,
60 especially at regional and global scales. On the other hand, satellite-based measurements, in
61 combination with ground-based measurements, can overcome many of these difficulties and
62 provide environmental data at multiple-scales (Seto 2007, 2011; Boucher and Seto 2009).

63 As mentioned earlier, the smart city approach requires collection of interdisciplinary data
64 and information from multiple sources and integration with modern technologies to provide a
65 new and cost-effective way for researchers and decision makers to study and manage cities. In
66 this book chapter, we introduce NASA satellite-based global and regional observations with
67 emphasis on the hydrologic cycle (e.g., precipitation, wind, temperature, soil moisture) for smart
68 cities. These products, consisting of both near-real-time and historical datasets, are publicly
69 available free of charge and can be used for global and regional research and applications.

Examples of using these datasets in smart cities are included. The chapter is organized as follows, first, a brief overview of NASA global satellite-based data products, followed by data services and tools, two examples of using satellite-based datasets in megacities, and finally summary and future plans.

2. **Overview of NASA Satellite-based Global Data Products for Smart Cities**

Significant progress has been made in satellite Earth's observations since the first successful launch of weather satellite, the Television Infrared Observation Satellite (TIROS), by NASA on April 1, 1960. In particular, NASA's Earth Observing System (EOS) is a coordinated series of polar-orbiting and low inclination satellites for long-term global observations of the land surface, biosphere, solid Earth, atmosphere, and oceans to enable an improved understanding of the Earth as an integrated system (NASA 2017a). At present, there are ~28 active satellite missions currently in space to provide observations to scientific and application users around the world (NASA 2017a). The Earth Observing System Data and Information System (EOSDIS) currently hosts ~22 PB of Earth Observation (EO) data at twelve DAACs (Distributed Active Archive Centers) and it is expected to grow rapidly over the coming years, to more than 37 (246 PB) PB by 2020 (2025) (NASA 2017b). Such large EO data archive is an important asset for environmental research and applications around the world including smart cities because the smart city approach requires multidisciplinary datasets collected from multiple sources.

NASA's EOS and other past NASA satellite mission data are available and distributed by the EOSDIS, with major facilities at twelve DAACs located throughout the United States (NASA 2017b). Scientific disciplines at twelve DAACs include atmosphere, cryosphere, human dimensions, land, ocean, calibrated radiance, solar radiance, etc. Table 1 lists the twelve DAACs

and their discipline-oriented data archives (NASA 2017b). For example, ocean winds and sea surface temperature data are available at the Physical Oceanography DAAC in the Jet Propulsion Laboratory (JPL). Lighting data from the NASA-JAXA Tropical Rainfall Measuring Mission (TRMM) are archived at the Global Hydrology Resource Center (GHRC) DAAC. As of this writing, a large collection of datasets and services are available at the twelve NASA data centers. However, due to page limit, it is difficult to give a detailed description for each DAAC. Here we focus on the Goddard Earth Sciences and Data and Information Services Center (GES DISC), located in Greenbelt, Maryland, USA, because it archives a large amount of interdisciplinary datasets in comparison to other DAACs. Datasets used in the examples in this article are archived at the GES DISC.

2.1. Satellite-based Data Products at the GES DISC

The GES DISC hosts global and regional satellite-based interdisciplinary data products from these scientific disciplines: precipitation, solar irradiance, atmospheric composition and dynamics, global modeling, etc. Currently, over 2700 unique data products are archived at the GES DISC and distributed to the public. Given such a large collection of products and space limitation, we can only present a brief overview of several major projects that are closely related to research and applications for smart cities.

2.1.1. Multi-satellite and Multi-sensor Merged Global Precipitation Products

Over the years, algorithms that utilize multi-satellites and multi-sensors (i.e., microwave and geostationary infrared sensors), or blended methods, have been developed to overcome a very limited spatial and temporal coverage from any single satellite (Adler et al. 2003; Huffman et al. 2007, 2009, 2010, 2012, 2013; Joyce et al. 2004; Mahrooghy et al. 2012; Hong et al. 2007, Sorooshian et al. 2000; Behrangi et al. 2009; Aonashi et al. 2009) and products are widely used

117 in hydrometeorological research and applications. For example, the TRMM Multi-Satellite
118 Precipitation Analysis (TMPA) products in Table 2 (Huffman et al. 2007, 2010, 2012, 2013),
119 developed by the Mesoscale Atmospheric Processes Laboratory at NASA Goddard Space Flight
120 Center, provide precipitation estimates at 3-hourly and monthly temporal resolutions on a 0.25-
121 degree x 0.25-degree grid available from January 1998 to present. The TMPA consists of two
122 products: near-real-time (3B42RT, spatial coverage: 60°N-60°S) and research-grade (3B42,
123 spatial coverage: 50°N-50°S). The former is less accurate, but provides quick precipitation
124 estimates suitable for near-real-time monitoring and modeling activities (e.g. Wu et al. 2012).
125 The latter, available approximately two months after observation, is calibrated with gauge data,
126 different sensor calibration, and additional post-processing in the algorithm. The resulting
127 product is more accurate and suitable for research (Huffman et al. 2007, 2010). Over the years,
128 the TMPA products have been widely used in various research and applications (e.g. Wu et al.
129 2012, Bitew et al. 2012, Gourley et al. 2011, Su et al. 2011, Gianotti et al. 2012, Tekeli 2017,
130 Engel et al. 2017, Tan and Duan 2017).

131 During the GPM era, the Integrated Multi-satellitE Retrievals for GPM (IMERG) product
132 suite (Huffman et al. 2017) not only addresses limited spatial and temporal coverage issues in
133 TRMM but also has been significantly improved comparing the TMPA products in terms of
134 spatial and temporal resolutions, i.e., from 0.25 degree to 0.1 degree and from 3-hourly to half-
135 hourly (Table 2). The IMERG suite contains of three output products, “Early satellites” (lag
136 time: ~6 hours), “Late satellites” (lag time: ~18 hours), and the final “Satellite-gauge” (lag time:
137 ~4 months) along with additional new input and intermediate files, creating a new opportunity
138 for research and applications. The retro-processing of the IMERG product suite back to the
139 TRMM era will be released in 2018.

2.1.2. Global and Regional Land Data Assimilation Products

Global and regional land data assimilation system data products include optimal fields of land surface states and fluxes (NASA 2017c). The fields are generated by ingesting satellite- and ground-based observational data products and using advanced land surface modeling and data assimilation techniques (NASA 2017c). A methodology is to implement a Land Data Assimilation System (LDAS) that consists of land-surface models (uncoupled from an atmospheric model). These land-surface models are forced with observations and thus the model results are not affected by Numerical Weather Prediction forcing biases (NASA 2017c). This research has been implemented using existing Surface Vegetation Atmosphere Transfer Schemes (SVATS) by NOAA, NASA/GSFC, NCAR, Princeton University, and the University of Washington at 1/8th-degree resolution across central North America and at 1/4th-degree resolution globally to evaluate these critical science questions (NASA 2017c). These LDAS systems have been run retrospectively starting in January 1979 and continue in near real-time, and are forced with gauge precipitation observations, satellite precipitation data, radar precipitation measurements, and output from numerical weather prediction models (NASA 2017c). Model parameters are derived from the existing high-resolution vegetation and soil coverages. The LDAS model results support water resources applications, numerical weather prediction studies, numerous water and energy cycle investigations, and also serve as a foundation for interpreting satellite and ground-based observations (NASA 2017c). Eventually, in situ or remotely-sensed observations (soil moisture, temperature, snow) of LDAS storages and fluxes (including evaporation, sensible heat flux, runoff) will be used to further validate and constrain the LDAS predictions using data assimilation techniques (NASA 2017c). The GES

DISC hosts the archive of data products from GLDAS, NLDAS, NCA-LDAS, and FLDAS (NASA 2017c).

2.1.3. Modern-Era Retrospective Analysis for Research and Applications (MERRA) Products

The Modern-Era Retrospective analysis for Research and Applications, Version 2 (MERRA-2), has been developed at the NASA Global Modeling and Assimilation Office (GMAO) at the NASA Goddard Space Flight Center (NASA 2017d). MERRA-2 provides global data beginning in 1980 and runs a few weeks behind real time (NASA 2017d). Alongside the meteorological data assimilation using a modern satellite database, MERRA-2 includes an interactive analysis of aerosols that feed back into the circulation, uses NASA's observations of stratospheric ozone and temperature (when available), and takes steps towards representing cryogenic processes (NASA 2017d). The MERRA project focuses on historical analyses of the hydrological cycle on a broad range of weather and climate time scales and places the NASA EOS suite of observations in a climate context (NASA 2017d). Compared to the previous version, advances have been made in the assimilation system that enables assimilation of modern hyperspectral radiance and microwave observations, along with GPS-Radio Occultation datasets (Riencker et al. 2011; Reichie and Liu 2014; Suarez and Bacmeister 2015; Takacs et al. 2015). MERRA-2 also includes advances in both the Goddard Earth Observing System Model, Version 5 (GEOS-5) and the GSI (Gridpoint Statistical Interpolation) assimilation system and NASA ozone observations after 2005. MERRA-2 begins from 1980 to present.

There are two types of precipitation parameters in MERRA-2: a) precipitation from the atmospheric model (variable PRECTOT in the MERRA-2 data collection) and b) observation-corrected precipitation (variable PRECTOTCORR; Reichle and Liu 2014; Bosilovich et al.

185 2015). Observational data are introduced in the latter parameter due to considerable errors that
186 propagate into land surface hydrological fields and beyond (Reichle et al. 2011).

187 Bosilovich et al. (2015) have conducted a general evaluation of MERRA-2 precipitation
188 estimates, including precipitation climatology, interannual variability, diurnal cycle, Madden-
189 Julian Oscillation (MJO) events, global water cycle and U.S. summertime variability. Major
190 findings (Bosilovich et al. 2015) are, 1) an overestimate of the modeled precipitation in the
191 tropical west Pacific Ocean, the eastern tropical ITCZ (the Intertropical Convergence Zone) and
192 the SPCZ (the South Pacific convergence zone) in DJF and JJA (Bosilovich et al. 2011, 2015); 2)
193 Extreme values of modeled precipitation in the vicinity of high topography in the tropics; 3) An
194 upward trend in the MERRA-2 time series exists and by contrast no trend is observed in GPCP
195 (the Global Precipitation Climatology Project); 4) Larger modeled precipitation diurnal cycle
196 (PDC) amplitude is found over the high mountains; 5) The phases of modeled PDC are not well
197 reproduced in several regions such as the U.S. Great Plains; 6) MJO signal from modeled
198 precipitation is stronger than GPCP; 7) MERRA-2 can reproduce the observed precipitation and
199 anomalies in U.S. summertime, reasonably well. Although the preliminary evaluation provides a
200 basic understanding of the MERRA-2 precipitation products, evaluation for extreme rainfall
201 events is missing and as a result, it is not clear about MERRA-2 precipitation behavior and
202 characteristics in extreme events.

203 The complete list of MERRA-2 products along with documentation and more is available
204 on the official MERRA-2 Web site (NASA 2017d). To facilitate data access, the GES DISC has
205 developed several data services and tools to be described in the next section.

206 **3. Data Services**

207 Although a large collection of NASA global satellite data is available for research and

applications around the world, many researchers find it challenging to discover, access, and use NASA satellite remote sensing data (Liu and Acker 2017). Heterogeneous data formats, complex data structures, large-volume data storage, special programming requirements, diverse analytical software options, and other factors often require a significant investment in time and resources, especially for novices (Liu and Acker 2017). Over the years, data services have been developed at NASA's EOSDIS DAACs to improve NASA data discovery and access. First, an EOSDIS Web search interface (NASA 2017e) has been developed and anyone, with a Web browser, can access NASA data products at twelve DAACs through this interface. Figure 2 is a screenshot of the EOSDIS Web search interface, showing a search box where users can type in a data variable name such as precipitation. User registration is required for downloading data from all EOSDIS data services. Users can also visit each individual DAAC and use their Web interfaces to access discipline-oriented data products and services. Furthermore, special discipline-oriented data tools have been developed at DAACs and they are organized in the following categories: Search and Order, Data Handling, Subsetting and Filtering, Geolocation, Reprojection, and Mapping, and Data Visualization & Analysis (NASA 2017f). EOSDIS DAACs also support Web services and various Web protocols for machine-to-machine data access and applications such as OPeNDAP (Open source Project for a Network Data Access Protocol), WMS (Web Map Service), GDS (GrADS Data Server), THREDDS, https, etc. To address data and science related issues and inquires from users, DAACs provide user services including Frequent Asked Questions (FAQs), data recipes, user forums, email or phone inquiry, etc. Due to space limitation, it is difficult to describe all data tools and services at the DAACs in one article. Since we focus on datasets for the hydrologic cycle in this article, data services at the GES DISC and other well-known services are presented.

3.1. Point-and-click Online Tools

Over the years, surveys (e.g. Kearns 2017) and experience from user support services at the GES DISC show that non-expert users and those who occasionally use satellite-based products prefer point-and-click data tools in order to obtain graphic and data assessment results. As mentioned above, new dataset assessment activities may not be straight-forward and can be costly. Point-and-click tools provide fast and easy access to satellite-based data products for all users without the need of coding and downloading data and software. Here, we introduce two popular point-and-click online tools developed by NASA: the NASA Worldview and the NASA GES DISC Giovanni.

3.1.1. NASA's Worldview

NASA’s Worldview is a tool developed by the NASA's EOSDIS project (Fig. 3). It provides the capability to interactively browse global, full-resolution satellite imagery and then download the underlying data (NASA 2017g). Worldview contains 400+ NASA satellite-based products and most of them are updated within three hours of observation, essentially showing the entire Earth as it looks "right now" (NASA 2017g). Worldview is a user-friendly online tool to support time-critical application areas such as wildfire management, air quality measurements, and flood monitoring. Mobile access is also available for Worldview. Worldview is powered by the Global Imagery Browse Services (GIBS) to rapidly retrieve its imagery for an interactive browsing experience (NASA 2017g). Data in Worldview images can be exported as several popular image formats such as JPEG and PNG. Image data in GeoTIFF and KMZ are also available. Figure 3 is a screenshot of Worldview, showing the Web interface and Hurricane Harvey in Gulf of Mexico on August 24, 2017. Hurricane Harvey made landfall near Corpus Christ, Texas, USA. A record-breaking flood in Houston, Texas was reported due to heavy

254 rainfall from Hurricane Harvey's rainbands. Fatalities and enormous economic loss in Houston
255 were reported as well.

256 **3.1.2. NASA GES DISC Giovanni**

257 Point-and-click tools can be further developed for in-depth data analysis and
258 visualization. A new infrastructure system, the Geospatial Interactive Online Visualization and
259 Analysis Infrastructure (Giovanni, NASA 2017h), has been developed by the GES DISC to assist
260 a wide range of users around the world with data access and evaluation, as well as with scientific
261 exploration and discovery (Liu and Acker 2017; Acker and Leptoukh 2007). There are 8
262 disciplines and 74 measurements available in Giovanni and they are listed in Tables 3 and 4,
263 respectively. Over 1800 variables are currently available in Giovanni as of this writing and more
264 are being added. Data variables in Giovanni are multi-missions and multi-disciplinary (Fig. 4).
265 Users can access these variables without downloading data and software (Liu and Acker 2017).
266 Over the years, a wide range of activities of using Giovanni has been reported by users, ranging
267 from classroom activities to scientific investigation. Over 1300 peer-reviewed papers across
268 various Earth science disciplines and other areas were published with help from Giovanni.

269 Giovanni has both Keyword and Faceted Search capabilities in its Web interface (Fig. 4)
270 for locating variables of interest. For example, a search for 'precipitation' returns over 100
271 related variables (Fig. 4). By using facets, one can filter for variables based on satellite missions
272 (TRMM, GPM), instruments, spatial or temporal resolution, etc.

273 Many commonly used analytical and plotting capabilities (Liu and Acker 2017), used to
274 capture spatial and temporal characteristics of datasets, are available in Giovanni. Mapping
275 options include time-averaging, animation, accumulation (precipitation), time-averaged overlay
276 of two datasets, and user-defined climatology. For time series, options include of area-averaged,

277 differences, seasonal, and Hovmöller diagrams. Cross-sections include latitude-pressure,
278 longitude-pressure, time-pressure, and vertical profile for 3-D datasets from AIRS (Atmospheric
279 Infrared Sounder) and MERRA. For data comparison, Giovanni has built-in processing code for
280 data sets that require measurement unit conversion and regridding. Commonly used comparison
281 functions include map and time-series differences, as well as correlation maps and X-Y scatter
282 plots (area-averaged or time-averaged). Zonal means and histogram distributions can also be
283 plotted. Samples of the analytical and plotting features are shown in Figs. 4 and 5.

284 Visualization features (Liu and Acker 2017) include interactive map area adjustment;
285 animation; interactive scatter plots; adjustments of data range; change of color palette;
286 contouring; and scaling (linear or log). The on-the-fly area adjustment feature allows an
287 interactive and detailed examination of a result map without re-plotting data. Animations are
288 helpful to track evolution of an event or seasonal changes. Interactive scatter plots allow
289 identification of the geolocation of a point of interest in a scatter plot. Adjustments of any of
290 these plots provide custom options to users.

291 To support increasing socioeconomic and GIS activities in Earth sciences, vector
292 shapefiles have been added for countries, states in the United States, and major watersheds
293 around the world. Available functions for shapefiles are time-averaged and accumulated maps,
294 area-averaged time series, and histogram. Land-sea masks have been recently added.

295 All data files involved in Giovanni processing are listed and available in the lineage page.
296 Available image formats are PNG, GEOTIFF, and KMZ (Keyhole Markup Language) that can
297 be used for different applications and software packages; for example, KMZ files can be
298 conveniently imported into Google Earth where a rich collection of overlays is available. All
299 input and output data are available in NetCDF, which can be handled by many off-the-shelf

300 software packages. Furthermore, users can bookmark URLs generated by Giovanni processing
301 for reference, documentation, or sharing with other colleagues.

302 **3.2. Data Rod Services**

303 Providing long time series data to the hydrology community can be a challenge (Teng et
304 al. 2012). In hydrology, earth surface features are expressed as discrete spatial objects such as
305 watersheds, river reaches, and point observation sites; and time varying data are contained in
306 time series associated with these spatial objects. Long-time histories of data may be associated
307 with a single point or feature in space. Most remote sensing precipitation products are expressed
308 as continuous spatial fields, with data sequenced in time from one data file to the next.
309 Hydrology tends to be narrow in space and deep in time, which poses a challenge during the
310 GPM era. For example, to generate a one-year time series, one needs to pull all the 0.1 deg., half-
311 hourly IMERG product, which can be time consuming and not suitable for online data services
312 due to the large volume of data.

313 The concept of data rods (Teng et al. 2012; Gallaher and Grant 2012; Rui et al. 2012,
314 2013) can be applied to this challenge. Teng et al. (2012) proposed two general solutions: 1)
315 retrieve multiple time series for short time periods and stitch the multiple time series into desired
316 single long time series and 2) reprocess (parameter and spatial subsetting) and archive data as
317 one-time cost approach. The resultant time series files would be geospatially searchable and
318 could be optimally accessed and retrieved by any user at any time (Teng et al. 2012). One
319 drawback for the data rod approach is that there are a lot of files to be generated and maintained.
320 For example, for IMERG, the number of files will be 1300 x 3600 = 4,680,000. At present, the
321 concept has been implemented in CUAHSI-HIS (Consortium of Universities for the
322 Advancement of Hydrologic Science, Inc. - Hydrologic Information System) and other

323 hydrologic community tools (Rui et al. 2013) where TMPA data time series data can be
324 accessed.

325 **3.3. Other Web Data Services**

326 NASA satellite-based data products at the GES DISC are also accessible (NASA 2017i)
327 via other Web services and protocols including https (the data archive), OPeNDAP, WMS, GDS,
328 etc. These protocols support for data downloading activities such as daily operations on the
329 user's side. The https method provides direct access to product archives. OPeNDAP, WMS,
330 GDS, etc. provide remote access to individual variables within datasets in a form usable by many
331 tools and software packages such as IDV, McIDAS-V, Panoply, Ferret, GrADS, etc. OPeNDAP
332 is a framework that simplifies all aspects of scientific data networking and makes local data
333 accessible to remote locations regardless of local storage format (OPeNDAP 2017). OPeNDAP
334 software is freely available to anyone. WMS is a standard Web protocol for serving
335 georeferenced map images over the Internet generated by a map server using data from a GIS
336 database and the specifications developed and published by the Open Geospatial Consortium
337 (OGC) in 1999 (WMS, 2017). The GDS, is a stable, secure data server that provides subsetting
338 and analysis services across the internet (GDS 2017). The core of the GDS is OPeNDAP, a
339 software framework used for data networking that makes local data accessible to remote
340 locations.

341 **4. Examples**

342 **4.1. The Pearl River Delta**

343 The Pearl River Delta (PRD) is located in Guangdong province, the People's Republic of
344 China (PRC). The PRD is a low-lying area surrounding the Pearl River estuary where the Pearl
345 River flows into the South China Sea (Wikipedia 2017a). The region has experienced an

346 economic boom and accelerated urbanization since the region was named as one of the three
347 Special Economic Zones (SEZs) by the PRC, and is one of the most densely urbanized regions in
348 the world (Wikipedia 2017a). The city of Guangzhou has become a mega city, the 3rd largest in
349 PRC and the largest in southern China, with a population of over 15 million. Adding the nearby
350 cities, the total population in PRD is over 40 million, forming the so-called the Pearl River Delta
351 Mega City. Figure 6 is the PRD viewed from the 2016 annual NASA black marble, a nighttime
352 view of the Earth derived from a composite of data from the Visible Infrared Imaging
353 Radiometer Suite (VIIRS) instrument on board the joint NASA/NOAA Suomi National Polar-
354 orbiting Partnership (Suomi NPP) satellite. UHI effect is also quite visible from the MODIS-
355 Terra monthly nighttime land-surface temperatures averaged between December 2016 and
356 February 2017 (Fig. 7). Giving economic activities at such scale, it is important to understand
357 environment impacts that are associated with economic activities and EO data play an important
358 role to provide such analysis and information. In this chapter, we present few examples regarding
359 how NASA EO datasets are used in this region.

360 **4.1.1. Typhoon Nida Rainfall**

361 Formed on July 28, 2016, Typhoon Nida struck the Philippines in late July and made
362 landfall in the PRD as a Category-1 typhoon (Fig. 8) in early August (Wikipedia 2017b).
363 According to news reports, Nida caused heavy economic loss in the affecting countries and
364 regions including the Philippines, the mainland of PRC, Hong Kong, and Vietnam (Wikipedia
365 2017b). In PRC alone, ~495,000 people in five southern provinces were affected and 37,000
366 required evacuation and 2,100 needed emergency assistances (Wikipedia 2017b). Homes and
367 crops were destroyed or damaged. People's lives in the region were severely disrupted,
368 according to news reports (Wikipedia 2017b).

NASA EO data are available for Nida. At the GES DISC, precipitation from TMPA, GPM, IMERG, MERRA, GLDAS, etc. with different spatial and temporal resolutions are available for research and analysis. Figure 8 is an example of total rainfall in mm accumulated between August 1-5, 2016. It is seen that heavy rainfall was received in the western part of the PRD and the heaviest rainfall area is found in the adjacent ocean off the coast of the PRD (Fig. 8). MERRA provides data such as wind, temperature, pressure, etc. for meteorological analysis. GLDAS provides data for hydrological research and analysis. Many of these datasets are available in the GES DISC Giovanni and ready for assessment, analysis, and visualization without the need to download data and software.

4.1.2. Atmospheric Composition Preliminary Analysis

As mentioned, the PRD has experienced an unprecedented economic growth and urbanization since 1979. The environmental conditions in the region have also experienced the changes, which requires EO data for research and analysis. MERRA uses various NASA satellite observations and the chemistry model to generate reanalysis products for research and applications. Figures 9 and 10 are the time series plots of sample MERRA-2 atmospheric chemistry variables for the PRD: monthly aerosol optical depth, SO2 surface mass concentration, CO surface concentration, and black carbon surface mass concentration, showing seasonal and inter-annual variations in the PRD over the past 30+ years. In Fig. 9, it is seen that aerosol optical depth experienced a large increasing trend since 2000, followed by a decreasing trend after mid-2000 or so. According to reports (Wikipedia 2017c), the PRD region's GDP in 2005 was ~US$221.2 billion, compared to US$89 billion in 2000. Further investigation is needed to better understand and link these observation results with the economic growth in the region. The SO2 surface mass concentration experienced a steady increase before 2000, followed a rapid

392 climb shortly after 2000 (Fig. 9). The increasing period ended near 2010 and the concentration
393 still remained high with fluctuations afterwards (Fig. 9). The similar trends are also found in CO
394 surface concentration (Fig. 10). The black carbon surface mass concentration (Fig. 10) is quite
395 similar to the aerosol optical depth in Fig. 9. It is necessary to point out that these time series
396 plots in Figs. 9 and 10 are preliminary and need to be verified independently with ground
397 measurements to ensure that biases and other issues are addressed properly.

398 **4.2. Estimation of Hurricane Contribution to Annual Precipitation in Maryland, USA**

399 The state of Maryland, USA is located in the Mid-Atlantic region near the nation's capital
400 or the Washington D.C. According the 2016 report (Censor Bureau 2016) from the U.S. Censor
401 Bureau, the population of the region that consists of Washington-Arlington-Alexandria and D.C.-
402 Virginia-Maryland-West Virginia, reached over 6 million in 2015 and became the 6th most
403 populous metro area in the U.S.

404 Despite the fact that major hurricanes (category 3 or above) rarely make landfall in the
405 state, Maryland is indirectly influenced by hurricane remnants (NOAA 2017a) such as rainfall.
406 Giving the global warming scenario, it is important to understand changes of hurricane size,
407 track and intensity since all of them could have significant impacts on precipitation in Maryland.
408 In this study, the TMPA precipitation products were used to assess hurricane precipitation.
409 Unlike many land-only precipitation products, the TMPA products not only provide precipitation
410 information over land but also over oceans, therefore, they are suitable for this type of study. The
411 objectives of this study are to estimate hurricane contribution to annual precipitation in Maryland
412 and its inter-annual variation (Liu and Liu 2015). The methodology could be applied to other
413 states or regions as well.

414 **4.2.1. Data and Methods**

415 The Version-7 3-hourly (3B42) and monthly (3B43) TMPA products are used in this
416 study. 3B42 and 3B43 provide a near-global (50° N-S) coverage of both land and oceans and
417 allow tracking of hurricane precipitation since some hurricanes can pass by Maryland over ocean
418 without making landfall and influence the state with rain, winds, waves, etc.

419 The TMPA algorithm (Huffman 1997; Huffman et al. 2007, 2010; Huffman and Bolvin
420 2014) consists of multiple independent precipitation estimates from the TMI (TRMM
421 Microwave Imager), Advanced Microwave Scanning Radiometer for Earth Observing Systems
422 (AMSR-E), Special Sensor Microwave Imager (SSMI), Special Sensor Microwave
423 Imager/Sounder (SSMIS), Advanced Microwave Sounding Unit (AMSU), Microwave Humidity
424 Sounder (MHS), microwave-adjusted merged geo-infrared (IR), and monthly accumulated rain
425 gauge analysis from the Global Precipitation Climate Centre (GPCC). The preprocessing
426 (Huffman and Bolvin 2014) of the TMPA products is as follows: (a) all input passive microwave
427 (PMW) products mentioned above are inter-calibrated to TRMM Combined Instrument (TCI)
428 precipitation estimates (TRMM product 3B31); (b) the IR estimates are computed using monthly
429 matched microwave-IR histogram matching; (c) then missing data in individual 3-hourly
430 merged-microwave fields are filled with the IR estimates. When the preprocessing is complete,
431 the 3-hourly multi-satellite fields are summed for the month and combined with the monthly
432 GPCC gauge analysis using inverse-error-variance weighting to form the best-estimate
433 precipitation rate and RMS precipitation-error estimates (Huffman and Bolvin 2014).

434 On April 15, 2015, TRMM was decommissioned after 17 years of continuously
435 collecting data from space. Although the TMPA is still in production using the remaining
436 satellites in the constellation, the changes and impact of the loss of TRMM on the TMPA
437 characteristics are expected to be small since TRMM only covers a band of 38° N-S and most of

438 Maryland is located north of this band. In addition, the use of gauge data from GPCC will correct
439 biases due to the loss of TRMM. The TMPA data between 1998 and 2013 are used in this study.
440 TMPA (Version 7) products were downloaded from the GES DISC (Liu et al. 2012).
441 There have been few processing issues (Huffman and Bolvin 2014) before, but all the TMPA
442 data used in this study are current.
443 Hurricane track data were obtained from the Best Track Data (HURDAT2), available at
444 the NOAA National Hurricane Center (NOAA 2017b). The radius for hurricane influence is set
445 to 500 km (Jiang and Zipser 2010), given typical
446 When tropical cyclones make landfall, they leave moist tropical and sub-tropical oceans
447 and enter drier land in mid-latitudes. As a result, water vapor as energy supply from underneath
448 is cut off and they quickly lose strength and become remnants. When the remnants interact with
449 frontal systems in mid-latitudes, rainfall is often enhanced when tropical warm and moist air
450 collides with cooler and drier air from north and extra lifting is generated. Meanwhile, it is
451 difficult to separate rainfall areas between tropical cyclones and frontal systems. In this study, we
452 do not attempt to separate the two rain regimes when they collide together. As long as the track
453 data are still available, rainfall within the 500-km radius is considered as hurricane rainfall (Jiang
454 and Zipser 2010).
455 The terrain of Maryland is characterized with the Appalachian Mountains in the west,
456 running through the panhandle (can obstruct passing cold fronts and cause rain shadow) and the
457 flat area in the east adjacent to the Atlantic Ocean (exposes area to coastal weather systems).
458 **4.1.1. Preliminary Results**
459 From 1998 to 2014, Hurricane Floyd, Charley, Ernesto, and Irene influenced the state of
460 Maryland. Our preliminary results from Fig. 11 show that Maryland experienced relatively high

amounts of precipitation in years 2003 and 2011 and relatively low amounts precipitation in the year 2001. In addition, further calculations show the average annual precipitation in Maryland is about 1200 mm/year. Figure 11 shows how much precipitation that hurricanes have contributed to annual precipitation. The highest contribution of precipitation (35%) occurred in 2011, due to major hurricanes passing through Maryland such as Hurricane Irene. Additionally, in 2001 when Maryland was experiencing a drought, no hurricanes passed through the state. The average contribution of precipitation by hurricanes to annual precipitation is about 15%. Figure 11 shows the average of the average annual precipitation compared against each year's precipitation with and without precipitation contributed by hurricanes. Results show that when precipitation contributed by hurricanes is removed, most annual precipitations fall below the average. Some exceptions occur such as in year 2003, where Maryland was receiving relatively high monthly precipitation in general throughout the year. As a result, one could conclude that precipitation contributed by hurricanes does affect Maryland's precipitation.

5. Summary and Future Plans

In this chapter, we introduce NASA satellite-based data and services with emphasis on the hydrologic cycle and data products at the GES DISC. Significant progress has been made in satellite Earth's observations since the first successful launch of weather satellite, TIROS, by NASA on April 1, 1960. In particular, NASA's EOS project is a coordinated series of polar-orbiting and low inclination satellites for long-term global observations of the land surface, biosphere, solid Earth, atmosphere, and oceans to enable an improved understanding of the Earth as an integrated system. NASA's EOS and other past NASA satellite mission data are available and distributed by the EOSDIS, with major facilities at twelve DAACs located throughout the United States. Science disciplines at twelve DAACs include atmosphere, cryosphere, human

484 dimensions, land, ocean, and calibrated radiance and solar radiance, etc. Datasets are emphasized
485 and used in the examples in this article are archived at the GES DISC.

486 The GES DISC hosts global and regional satellite-based data products from these science
487 disciplines: precipitation, solar irradiance, atmospheric composition and dynamics, global
488 modeling, etc. There are over 2700 unique data products archived at the GES DISC. In this
489 chapter, we only present several major projects that are closely related to smart cities.

490 Multi-satellite and multi-sensor merged global precipitation products are available at the
491 GES DISC. In particular, The IMERG suite contains of three output products, “Early satellites”
492 (lag time: ~4 hours), “Late satellites” (lag time: ~18 hours), and the final “Satellite-gauge” (lag
493 time: ~2 months) along with additional new input and intermediate files. The retro-processing of
494 the IMERG product suite back to the TRMM era will be released in late 2018.

495 Global and regional land data assimilation system data products include optimal fields of
496 land surface states and fluxes. They are generated by ingesting satellite- and ground-based
497 observational data products and using advanced land surface modeling and data assimilation
498 techniques. Both forcing data and model results support water resources applications, numerical
499 weather prediction studies, numerous water and energy cycle investigations, and also serve as a
500 foundation for interpreting satellite and ground-based observations.

501 The Modern-Era Retrospective analysis for Research and Applications, Version 2
502 (MERRA-2), has been developed at the NASA Global Modeling and Assimilation Office
503 (GMAO) at the NASA Goddard Space Flight Center. MERRA-2 provides global data beginning
504 in 1980 and runs a few weeks behind real time. Alongside the meteorological data assimilation
505 using a modern satellite database, MERRA-2 includes an interactive analysis of aerosols that
506 feed back into the circulation, uses NASA's observations of stratospheric ozone and temperature

(when available), and takes steps towards representing cryogenic processes. The MERRA project focuses on historical analyses of the hydrological cycle on a broad range of weather and climate time scales and places the NASA EOS suite of observations in a climate context.

Two popular point-and-click tools are presented. First, NASA's Worldview provides the capability to interactively browse global, full-resolution satellite imagery and then download the underlying data (NASA 2017g). Worldview contains 400+ NASA satellite-based products and most of them are updated within three hours of observation, essentially showing the entire Earth as it looks "right now" (NASA 2017g). On the other hand, NASA's GES DISC Giovanni is designed for in-depth data analysis and visualization. There are 8 disciplines and 74 measurements available in Giovanni and they are listed in Tables 3 and 4, respectively. Over 1700 variables are currently available in Giovanni as of this writing and more are being added. Data variables in Giovanni are multi-disciplinary and users can access them without downloading data and software (Liu and Acker 2017). Over the years, a wide range of activities of using Giovanni has been reported by users, ranging from classroom activities to scientific investigation. Over 1300 peer-reviewed papers across various Earth science disciplines and other areas were published with help from Giovanni.

NASA satellite-based data products at the GES DISC are also accessible (NASA 2017i) via other Web services and protocols including https (the data archive), OPeNDAP, WMS, GDS, etc.

Two examples were presented regarding the use of satellite-based data products in understanding environment changes and conditions in megacities. In Example 1, the TMPA precipitation dataset was presented with the accumulated rainfall map for Typhoon Nida that made landfall in the PRD region. Time series plots of several atmospheric composition datasets

530 from MERRA-2 were plotted and analyzed, showing significant changes in the atmospheric
531 environment in PRD, which could be associated with the unprecedented economic growth and
532 urbanization in the region, especially since 2000. It is necessary to mention that these
533 preliminary results need to be verified independently with ground or other measurements to
534 address biases and other issues.

535 In Example 2, the effect of hurricanes on annual precipitation in Maryland was
536 investigated. From 1998 to 2014, Hurricane Floyd, Charley, Ernesto, and Irene influenced the
537 state of Maryland. Our preliminary results from Fig. 11 show that Maryland experienced
538 relatively high amounts of precipitation in years 2003 and 2011 and relatively low amounts
539 precipitation in the year 2001. In addition, further calculations show the average annual
540 precipitation in Maryland is about 1200 mm/year. Figure 11 shows how much precipitation
541 hurricanes have contributed to annual precipitation. The highest contribution of precipitation
542 (35%) occurred in 2011, possibly due to major hurricanes passing through Maryland such as
543 Hurricane Irene. Additionally, in 2001 when Maryland was experiencing a drought, no
544 hurricanes passed through the state. The average contribution of precipitation by hurricanes to
545 annual precipitation is about 15%. Figure 11 shows the average of the average annual
546 precipitation compared against each year's average precipitation with and without precipitation
547 contributed by hurricanes. Results show that when precipitation contributed by hurricanes is
548 removed, most annual precipitations fall below the average for each. Some exceptions occur
549 such as in year 2003, where Maryland was receiving relatively high monthly precipitation in
550 general. As a result, one could conclude that precipitation contributed by hurricanes does affect
551 Maryland's precipitation.

As of this writing, EOSDIS hosts ~22 PB of Earth Observation (EO) data at twelve DAACs and it is expected to grow to more than 37 (246 PB) PB by 2020 (2025) (NASA 2017a). Such large EO data archive is an important asset for environmental research and applications around the world. Over the years, NASA EOSDIS has developed data services and tools to facilitate data discovery and access in twelve discipline-oriented DAACs. For complex issues of smart cities, it often requires a multi-disciplinary approach which needs an information system that can integrate all these data products archived at twelve DAACs as well as other related data products from users, providing a one-stop shop for data and services by removing obstacles such as data discovery, access, interoperability, etc. and better address environmental issues encountered in city planning, operations, research, etc. (Güneralp and Seto 2008). The NASA GES DISC Giovanni is an example that makes multi-discipline data variables available in one place and efforts are being carried out to include additional datasets from other DAACs and make them available in Giovanni. The ongoing NASA EOSDIS Cloud Evolution Project (NASA 2017j) will have the potential for developing an information system that supports multi-disciplinary data products and services. Moving from discipline-oriented to multi-discipline-oriented data services is not a simple task, which will involve in a team of data scientists from NASA and other organizations as well as from end users of smart cities due to many obstacles to be overcome such as data formats, data volume, data structures, terminology in different disciplines, etc. Nonetheless, still a lot of work needs to be done to develop better information systems and services for efficiently solving problems in smart cities.

Acknowledgements

We recognize the team effort of all past and current members at the GES DISC for their contributions to the development of data services and tools such as Giovanni. We extend our

thanks to data set algorithm developers and many users for their feedback and suggestions. The GES DISC is funded by NASA's Science Mission Directorate (SMD).

References:

Acker, J. G., and G. Leptoukh, 2007: Online analysis enhances use of NASA earth science data. *Eos. Trans. Amer. Geophys. Union*, ***88*** *(2)*, 14–17.

Adler, R.F., G.J. Huffman, A. Chang, R. Ferraro, P. Xie, J. Janowiak, B. Rudolf, U. Schneider, S. Curtis, D. Bolvin, A. Gruber, J. Susskind, P. Arkin, E. Nelkin 2003: The Version 2 Global Precipitation Climatology Project (GPCP) Monthly Precipitation Analysis (1979-Present). *J. Hydrometeor.*, **4**, 1147-1167.

Aonashi, K., J. Awaka, M. Hirose, T. Kozu, T. Kubota, G. Liu, S. Shige, S. Kida, S. Seto, N. Takahashi, and Y. N. Takayabu, 2009: GSMaP passive, microwave precipitation retrieval algorithm: Algorithm description and validation. J. Meteor. Soc. Japan, 87A, 119-136.

Behrangi, A., K.-L. Hsu, B. Imam, S. Sorooshian, G. J. Huffman, and R. J. Kuligowski, 2009: PERSIANN-MSA: A Precipitation Estimation Method from Satellite-Based Multispectral Analysis. *J. Hydrometeor*, **10**, 1414–1429. doi: http://dx.doi.org/10.1175/2009JHM1139.1

Bitew, M., M., M. Gebremichael, L. T. Ghebremichael, and Y. A. Bayissa, 2012: Evaluation of High-Resolution Satellite Rainfall Products through Streamflow Simulation in a Hydrological Modeling of a Small Mountainous Watershed in Ethiopia. *J. Hydrometeor*, **13**, 338–350. doi: http://dx.doi.org/10.1175/2011JHM1292.1

Bosilovich, M., S. Akella, L. Coy, R. Cullather, C. Draper, R. Gelaro, R. Kovach, Q. Liu, A. Molod, P. Norris, K. Wargan, W. Chao, R. Reichle, L. Takacs, Y. Vikhliaev, S. Bloom, A. Collow, S. Firth, G. Labow, G. Partyka, S. Pawson, O. Reale, S. Schubert, and M. Suarez, 2015. Techincal Report Series on Global Modeling and Data Assimilation, Vol. 43, R. Koster, Edtor. Available online: http://gmao.gsfc.nasa.gov/pubs/tm/docs/Bosilovich803.pdf

Boucher, A. and K. C. Seto, 2009. "Methods and Challenges for Using High-Temporal Resolution Data to Monitor Urban Growth." *Global Mapping of Human Settlements: Experiences, Data Sets, and Prospects.* Ed. P. Gamba and M. Herold. Boca Raton, Florida: CRC Press, 2009. 339+.

Census Bureau, 2016, Four Texas Metro Areas Collectively Add More Than 400,000 People in

the Last Year, Census Bureau Reports, available online, https://www.census.gov/newsroom/press-releases/2016/cb16-43.html, last accessed, September 6, 2017.

Engel T., Fink A.H., Knippertz P., Pante G. and Bliefernicht J., 2017. Extreme precipitation in the West African cities of Dakar and Ouagadougou-atmospheric dynamics and implications for flood risk assessments. Journal of Hydrometeorology, 18: 2937-2957.

Gallaher, D. and G. Grant, 2012, Data Rods: High speed, time-series analysis of massive cryospheric data sets using pure object databases, Geoscience and Remote Sensing Symposium (IGRASS), 22-27 July 2012 [available: http://ieeexplore.ieee.org/xpl/articleDetails.jsp?reload=true&arnumber=6352413&contentType=Conference+Publications]

GDS, 2017, The GrADS Data Server (GDS), available online, http://cola.gmu.edu/grads/gds.php, last accessed, September 6, 2017.

Gianotti, R. L., D. Zhang, and E. A. B. Eltahir, 2012: Assessment of the Regional Climate Model Version 3 over the Maritime Continent Using Different Cumulus Parameterization and Land Surface Schemes. *J. Climate*, **25**, 638–656. doi: http://dx.doi.org/10.1175/JCLI-D-11-00025.1

Gourley, J. J., Y. Hong, Z. L. Flamig, J. Wang, H. Vergara, and E. N. Anagnostou, 2011: Hydrologic Evaluation of Rainfall Estimates from Radar, Satellite, Gauge, and Combinations on Ft. Cobb Basin, Oklahoma. *J. Hydrometeor*, **12**, 973–988. doi: http://dx.doi.org/10.1175/2011JHM1287.1

Güneralp, B. and K. C. Seto, 2008. "Environmental impacts of urban growth from an integrated dynamic perspective: A case study of Shenzhen, South China." Global Environmental Change 18.4 (2008): 720-735. DOI: doi:10.1016/j.gloenvcha.2008.07.004

Guo, J.-P., and Coauthors, 2016: Delaying precipitation and lightning by air pollution over Pearl River Delta. Part I: Observational analyses. J. Geophys. Res. Atmos., 121, 6472–6488, doi:https://doi.org/10.1002/2015JD023257.

Hong, Y., D. Gochis, J. Cheng, K.-L. Hsu, S. Sorooshian, 2007: Evaluation of PERSIANN-CCS Rainfall Measurement Using the NAME Event Rain Gauge Network. *J. Hydrometeor*, **8**, 469–482. doi: http://dx.doi.org/10.1175/JHM574.1

644 Huffman, G.J., R.F. Adler, D.T. Bolvin, G. Gu, E.J. Nelkin, K.P. Bowman, Y. Hong, E.F.
645 Stocker, D.B. Wolff, 2007: The TRMM Multi-satellite Precipitation Analysis: Quasi-Global,
646 Multi-Year, Combined-Sensor Precipitation Estimates at Fine Scale. *J. Hydrometeor.*, 8(1), 38-
647 55.
648
649 Huffman, G.J, R.F. Adler, D.T. Bolvin, G. Gu 2009: Improving the Global Precipitation Record:
650 GPCP Version 2.1. *Geophys. Res. Lett.*, **36**,L17808, doi:10.1029/2009GL040000.
651
652 Huffman, G.J., R.F. Adler, D.T. Bolvin, E.J. Nelkin, 2010: The TRMM Multi - satellite
653 Precipitation Analysis (*TAMPA*). Chapter 1 in Satellite Rainfall Applications for Surface
654 Hydrology , F. Hossain and M. Gebremichael, Eds. Springer Verlag, ISBN: 978-90-481-2914-0,
655 3-22.
656
657 Huffman, G.J. and D.T. Bolvin, 2012: Real-Time TRMM Multi-Satellite Precipitation Analysis
658 Data Set Documentation. Available online:
659 ftp://trmmopen.gsfc.nasa.gov/pub/merged/V7Documents/3B4XRT_doc_V7.pdf (accessed on 8
660 June 2014).
661
662 Huffman, G.J. and D.T. Bolvin, 2013: TRMM and Other Data Precipitation Data Set
663 Documentation. Available online: ftp://meso-
664 a.gsfc.nasa.gov/pub/trmmdocs/3B42_3B43_doc.pdf (accessed on September 6, 2017).
665
666 Huffman, G.J. and D.T. Bolvin, 2014, "TRMM and Other Data Precipitation Data Set
667 Documentation," available at: ftp://meso-a.gsfc.nasa.gov/pub/trmmdocs/3B42_3B43_doc.pdf,
668 accessed on September 6, 2017.
669
670 Huffman, G.J., D. Bolvin, D. Braithwaite, K. Hsu, R. Joyce, C. Kidd, E. Nelkin, S. Sorooshian,
671 J. Tan, P. Xie, 2017, IMERG Algorithm Theoretical Basis Document (ATBD), Available online:
672 https://pmm.nasa.gov/sites/default/files/document_files/IMERG_ATBD_V4.6.pdf, last accessed:
673 September 6, 2017.
674
675 Jiang, H., and E. J. Zipser, 2010: Contribution of tropical cyclones to the global precipitation
676 from eight seasons of TRMM data: Regional, seasonal, and interannual variations. *J. Climate*,
677 **23**, 1526–1543, doi:10.1175/2009JCLI3303.1.
678

679 Jin, M., Wittaya Kessomkiat and Gary Pereira, 2011: Satellite-Observed Urbanization Characters
680 in Shanghai, China: Aerosols, Urban Heat Island Effect, and Land-Atmosphere Interactions,
681 Remote Sensing 2011, 3, 83-99; doi:10.3390/rs3010083
682
683 Jin, M., J. M. Shepherd, and W. Zheng, 2010: Urban Surface Temperature Reduction via the
684 Urban Aerosol Direct Effect ------A Remote Sensing and WRF Model Sensitivity Study PDF file
685 of the paper Advances in Meteorology Volume 2010 (2010), Article ID 681587, 14
686 pagesdoi:10.1155/2010/681587
687
688 Jin, M., J. M. Shepherd, M. D. King, 2005: Urban aerosols and their interaction with clouds and
689 rainfall: A case study for New York and Houston. J. Geophysical Research, 110, D10S20,
690 doi:10.1029/2004JD005081.
691
692 Joyce, R. J., J. E. Janowiak, P. A. Arkin, and P. Xie, 2004: CMORPH: A method that produces
693 global precipitation estimates from passive microwave and infrared data at high spatial and
694 temporal resolution.. J. Hydromet., 5, 487-503.
695
696 Kaufmann, R. K., K. C. Seto, A. Schneider, L. Zhou, Z. Liu, and W. Wang. “Climate Response
697 to Rapid Urban Growth: Evidence of a Human-Induced Precipitation Deficit.” Journal of
698 Climate 20.10 (2007): 2299-2306. DOI: 10.1175/JCLI4109.1
699
700 Kearns, E. 2017, Improving Access to Open Data through NOAA’s Big Data Project, available
701 online: https://bigdatawg.nist.gov/Day2_08_NIST_Big_Data-Kearns.pdf, last accessed,
702 September 6, 2017.
703
704 Lee, T., S. Miller, F. Turk, C. Schueler, R. Julian, S. Deyo, P. Dills, and S. Wang, 2006: The
705 NPOESS VIIRS Day/Night Visible Sensor. Bull. Amer. Meteor. Soc., 87, 191–199, doi:
706 10.1175/BAMS-87-2-191
707
708 Liu, Z. and J. Acker, 2017, Giovanni: The bridge between data and science, Eos, 98,
709 https://doi.org/10.1029/2017EO079299. Published on 24 August 2017.
710
711 Liu, Z., D. Ostrenga, B. Vollmer, et al. 2017. "Global Precipitation Measurement Mission
712 Products and Services at the NASA GES DISC." Bulletin of the American Meteorological
713 Society, 98 (3): 437-444 [10.1175/bams-d-16-0023.1]
714
715 Liu, J. and Z. Liu, 2015, The Connection Between Hurricanes and Precipitation in Maryland, in

716 Global Precipitation Measurement, Validation, and Applications III, AGU Fall Meeting, San
717 Francisco, 14-18 December 15.
718
719 Liu, Z., D. Ostrenga, W. Teng, and S. Kempler, 2012: Tropical Rainfall Measuring Mission
720 (TRMM) Precipitation Data and Services for Research and Applications. Bulletin of the
721 American Meteorological Society, doi: http://dx.doi.org/10.1175/BAMS-D-11-00152.1
722
723 Mahrooghy, M., V. G. Anantharaj, N. H. Younan, J. Aanstoos, K.-L. Hsu, 2012: On an
724 Enhanced PERSIANN-CCS Algorithm for Precipitation Estimation. *J. Atmos. Oceanic Technol.*,
725 **29**, 922–932. doi: http://dx.doi.org/10.1175/JTECH-D-11-00146.1
726
727 NASA, 2017a, NASA's Earth Observing System Project Science Office, available online,
728 https://eospso.gsfc.nasa.gov/, last accessed, September 6, 2017.
729
730 NASA, 2017b, NASA Earth Science Data and Information System Project, available online,
731 https://earthdata.nasa.gov/about/esdis-project, last accessed, September 6, 2017.
732
733 NASA, 2017c, Land Data Assimilation Systems, available online,
734 https://ldas.gsfc.nasa.gov/gldas/, last accessed, September 6, 2017.
735
736 NASA, 2017d, Modern-Era Retrospective analysis for Research and Applications, Version 2,
737 available online, https://gmao.gsfc.nasa.gov/reanalysis/MERRA-2/, last accessed, September 6,
738 2017.
739
740 NASA, 2017e, Earthdata Search, available online, https://search.earthdata.nasa.gov/search, last
741 accessed, September 6, 2017.
742
743 NASA, 2017f, EOSDIS Data Tools, available online, https://earthdata.nasa.gov/earth-
744 observation-data/tools, last accessed, September 6, 2017.
745
746 NASA, 2017g, NASA Worldview, available online, https://worldview.earthdata.nasa.gov/, last
747 accessed, September 6, 2017.
748
749 NASA, 2017h, NASA GES DISC Giovanni, available online, https://giovanni.gsfc.nasa.gov/,
750 last accessed, September 6, 2017.
751

NASA, 2017i, Web Services at GES DIC, available online, https://disc.gsfc.nasa.gov/information/tools?title=OPeNDAP%20and%20GDS, last accessed, September 6, 2017.

NASA, 2017j, EOSDIS Cloud Evolution, available online, https://earthdata.nasa.gov/about/eosdis-cloud-evolution, last accessed, September 6, 2017.

NOAA, 2017a, Historical Hurricane Tracks, available online, https://csc.noaa.gov/hurricanes/, last accessed, September 6, 2017.

NOAA, 2017b, Hurricane Best Track Data, available online, http://www.nhc.noaa.gov/data/, last accessed, September 6, 2017.

OPeNDAP, 2017, OPeNDAP – Advanced Software for Remote Data Retrieval, available online, https://www.opendap.org/, last accessed, September 6, 2017.

Reichle, R. H., and Q. Liu, 2014. Observation-Corrected Precipitation Estimates in GEOS-5. NASA/TM–2014-104606, Vol. 35.

Rienecker, M.M., M.J. Suarez, R. Gelaro, R. Todling, J. Bacmeister, E. Liu, M.G. Bosilovich, S.D. Schubert, L. Takacs, G.-K. Kim, S. Bloom, J. Chen, D. Collins, A. Conaty, A. da Silva, et al. (2011), MERRA: NASA's Modern-Era Retrospective Analysis for Research and Applications. J. Climate, 24, 3624-3648, doi:10.1175/JCLI-D-11-00015.1.

Rui, H., R. Strub, W.L. Teng, B. Vollmer, D.M. Mocko, D.R. Maidment, and T.L. Whiteaker, 2013. Enhancing access to and use of NASA earth sciences data via CUAHSI-HIS (Hydrologic Information System) and other hydrologic community tools, AGU Fall Meeting, San Francisco, CA, Dec. 9-13, 2013.

Rui, H., B. Teng, R. Strub, and B. Vollmer, 2012. Data reorganization for optimal time series data access, analysis, and visualization, AGU Fall Meeting, San Francisco, CA, Dec. 3-7, 2012.

Seto, K. C., 2011, Monitoring Urban Growth and Its Environmental Impacts Using Remote Sensing: Examples from China and India. Global Urbanization. Ed. E. Birch and S. Wachter. Philadelphia: University of Pennsylvania Press, 2011. 151-166.

Seto, K. C. and J. M. Shepherd. “Global urban land-use trends and climate impacts.” Current Opinion in Environmental Sustainability 1.1 (2009): 89-95. DOI: doi:10.1016/j.cosust.2009.07.012

786 Seto, K. C. “Urbanization in China: The Pearl River Delta Example.” Our Changing Planet: The
787 View From Space. Ed. M. D. King, C. L. Parkinson, K. C. Partington, and R. G. Williams.
788 Cambridge: Cambridge University Press, 2007.

789 Shepherd, M. J. and M. Jin 2004: Linkages between the Urban Environment and Earth's Climate
790 System. EOS, 85, 227-228

791 Su, Fengge, Huilin Gao, George J. Huffman, Dennis P. Lettenmaier, 2011: Potential Utility of
792 the Real-Time TMPA-RT Precipitation Estimates in Streamflow Prediction. *J. Hydrometeor*, **12**,
793 444–455. doi: http://dx.doi.org/10.1175/2010JHM1353.122. Prat, Olivier P., Brian R.
794 Nelson, 2013: Precipitation Contribution of Tropical Cyclones in the Southeastern United States
795 from 1998 to 2009 Using TRMM Satellite Data. *J. Climate*, **26**, 1047–1062. doi:
796 http://dx.doi.org/10.1175/JCLI-D-11-00736.1
797
798 Suarez, M., and Bacmeister, J., 2015: Development of the GEOS-5 atmospheric general
799 circulation model: evolution from MERRA to MERRA2, Geosci. Model Dev., 8, 1339-1356,
800 doi:10.5194/gmd-8-1339-2015.

801 Takacs, L. L., M. Suarez, and R. Todling, 2015. Maintaining Atmospheric Mass and Water
802 Balance Within Reanalysis. NASA/TM–2014-104606, Vol. 37

803 Tan, M.L.; Duan, Z. Assessment of GPM and TRMM Precipitation Products over Singapore.
804 *Remote Sens.* **2017**, *9*, 720.
805
806 Tekeli, A.E. Exploring Jeddah Floods by Tropical Rainfall Measuring Mission Analysis. *Water*
807 **2017**, *9*, 612.
808

809 Teng, B., Maidment, D.R., Vollmer, B., Peters-Lidard, C., Rui, H., Strub, R., Whiteaker, T.,
810 Mocko, D., and Kirschbaum, D. (2012) Bridging the digital divide between discrete and
811 continuous space-time array data to enhance accessibility to and usability of NASA Earth
812 Sciences data for the hydrological community. AGU Fall Meeting, December 3-7, San
813 Francisco, CA.

814 United Nations, 2014, "World Urbanization Prospects," Available in,
815 https://esa.un.org/unpd/wup/Publications/Files/WUP2014-Highlights.pdf
816
817 Wikipedia, 2017a, The Pearl River Delta, available online:
818 https://en.wikipedia.org/wiki/Pearl_River_Delta, last accessed, September 6, 2017.
819
820 Wikipedia, 2017b, Tropical Storm Nida (2016), available online:

https://en.wikipedia.org/wiki/Tropical_Storm_Nida_(2016), last accessed, September 6, 2017.

Wikipedia, 2017c, Pearl River Delta Economic Zone, available online, https://en.wikipedia.org/wiki/Pearl_River_Delta_Economic_Zone, last accessed, September 6, 2017.

WMS, 2017, Web Map Service, available online, https://en.wikipedia.org/wiki/Web_Map_Service, last accessed, September 6, 2017.

Wu H., R. F. Adler, Y. Hong, Y. Tian, and F. Policelli, 2012: Evaluation of Global Flood Detection Using Satellite-Based Rainfall and a Hydrologic Model. J. Hydrometeor, 13, 1268.1284.

Zhang, H. M. Jin, M. Leach, 2017: A Study of the Oklahoma City Urban Heat Island Effect Using a WRF/Single-Layer Urban Canopy Model, a Joint Urban 2003 Field Campaign, and MODIS Satellite Observations. Climate 2017, in print.

839 **Table 1**. EOSDIS DAACs and their archived products (NASA 2017b).

Distributed Active Archive Center (DAAC)	Data Products
Alaska Satellite Facility (ASF) DAAC	SAR products, sea ice, polar processes, geophysics, etc.
Atmospheric Science Data Center (ASDC)	Radiation budget, clouds, aerosols, tropospheric chemistry, etc.
Crustal Dynamics Data Information System (CDDIS)	Space geodesy, solid Earth, etc.
Global Hydrology Resource Center (GHRC) DAAC	Hydrologic cycle, severe weather interactions, lightning, atmospheric convection, etc.
Goddard Earth Sciences Data and Information Services Center (GES DISC)	Global precipitation, solar irradiance, atmospheric composition and dynamics, global modeling, etc.
Land Processes DAAC (LP DAAC)	Surface reflectance, land cover, vegetation indices, etc.
Level 1 and Atmosphere Archive and Distribution System (LAADS) DAAC	MODIS and VIIRS Level-1 and atmosphere data products
National Snow and Ice Data Center (NSIDC) DAAC	Snow and ice, cryosphere, climate interactions, sea ice, etc.
Oak Ridge National Laboratory (ORNL) DAAC	Biogeochemical dynamics, ecological data, environmental processes, etc.
Ocean Biology DAAC (OB.DAAC)	Ocean biology, sea surface temperature, etc.
Physical Oceanography DAAC (PO.DAAC)	Gravity, sea surface temperature, ocean winds, topography, circulation and currents, etc.
Socioeconomic Data and Applications Data Center (SEDAC)	Human interactions, land use, environmental sustainability, geospatial data, etc.

840

841 **Table 2.** Global gridded multi-sensor and multi-satellite precipitation products (Liu et al. 2012,
842 2017).

Dataset	Description	Date Range	Spatial Resolution and coverage	Temporal Resolution
The Integrated Multi-satellitE Retrievals for GPM (IMERG) – "Early, Late, and Final"	Rain rate from multi-satellite, multi-sensor and gauge measurements	1998-01-01 - present	Gridded 10 km, global, initially 60°N-60°S	Half-hourly, daily, and monthly
TRMM Multi-satellite Precipitation Analysis (Near-real-time, Research)	Rain rate from multi-satellite and multi-sensor measurements	1998-01-01 - present	Gridded 25 km, 60°N-60°S (Research: 50°N-50°S)	3-hourly, daily and monthly

843 **Table 3.** Disciplines and variables in Giovanni (NASA 2017h).

Disciplines (No. of Variables)
Aerosols (183)
Atmospheric Chemistry (79)
Atmospheric Dynamics (385)
Cryosphere (15)
Hydrology (997)
Ocean Biology (44)
Oceanography (48)
Water and Energy Cycle (1065)

844

845 **Table 4.** Measurements and variables in Giovanni (NASA 2017h).

Measurement (No. of Variables)							
Aerosol Index (3)	Buoyancy (2)	Dust (23)	Height, Level (12)	OLR (19)	Runoff (63)	Soil Temperature (105)	Water Storage (1)
Aerosol Optical Depth (83)	CH4 (16)	Emissivity (4)	Incident Radiation Anomaly (2)	Organic Carbon (8)	SO2 (4)	Statistics (24)	Wind Stress Magnitude (4)
Air Pressure Anomaly (1)	CO (21)	Energy (12)	Incident Radiation (70)	Ozone (28)	SO4 (4)	Streamflow (1)	Wind Velocity (7)
Air Pressure (51)	CO2 (2)	Erythemal UV (4)	Iron (2)	Particulate Matter (42)	Scattering Angle (4)	Surface Runoff (1)	Wind (72)
Air Temperature (84)	Canopy Water Storage (6)	Evaporation Anomaly (1)	Irradiance (6)	Phytoplankton (16)	Sea Salt (5)	Surface Temperature (55)	
Albedo (21)	Chlorophyll (11)	Evaporation (44)	Latent Heat Flux (5)	Precipitation Anomaly (2)	Sea Surface Temperature (3)	Total AOD Climatology Anomaly (6)	
Altitude (8)	Cloud Fraction (32)	Evapotranspiration (41)	Latent Heat (1)	Precipitation (107)	Sensible Heat Flux (5)	Total Aerosol Optical Depth (49)	
Angstrom Exponent (17)	Cloud Properties (75)	Flooding (3)	Mixed Layer Depth (2)	Quality Info (1)	Sensible Heat (1)	UV Exposure (1)	
Atmospheric Moisture (114)	Component Aerosol Optical Depth (7)	Geopotential (11)	NO2 (2)	Radiation, Net (56)	Snow/Ice (37)	Vegetation (9)	
Black Carbon (5)	Diffusivity (1)	Heat Flux (102)	Nitrate (2)	Reflectivity (25)	Soil Moisture (203)	Vorticity (2)	

Figure captions:

Figure 1. Cities in Asia viewed from the 2016 annual NASA black marble, a nighttime view of the Earth , derived from a composite of data from the Visible Infrared Imaging Radiometer Suite (VIIRS) instrument on board the joint NASA/NOAA Suomi National Polar-orbiting Partnership (Suomi NPP) satellite (Lee et al. 2006). (Credit: NASA Worldview).

Figure 2. NASA Earthdata (NASA 2017b) provides a Web interface for searching and accessing NASA data at twelve EOSDIS DAACs.

Figure 3. The NASA Worldview Web interface (NASA 2017g) showing Hurricane Harvey in Gulf of Mexico on August 24, 2017.

Figure 4. Top: The Web portal of NASA GES DISC Giovanni (NASA 2017h) with many features for easy locating a variable of interest, data analysis, and visualization; Middle: Corrected reflectance (true color) from MODIS Aqua on September 4, 2017, showing smoke from forest fires spreads across the United States and Canada (More detailed story is available at, https://earthobservatory.nasa.gov/IOTD/view.php?id=90899). Bottom: The combined dark target and deep blue aerosol optical depth (AOD) at 0.55 micron for land and ocean from MODIS Aqua on September 4, 2017. Combined with NASA Worldview, Giovanni provides analysis and visualization of the smoke aerosol for the event.

Figure 5. Sample graphics from Giovanni. Top: Accumulated rainfall (the GPM IMERG Late Run daily product) in mm from Hurricane Harvey (see Fig. 3) in Houston, Texas between August 21-31, 2017. Bottom: Time series of area averaged daily accumulated precipitation (mm/day) in Houston.

Figure 6. Similar to Fig. 1, except for the Pearl River Delta.

Figure 7. Map of MODIS-Terra monthly nighttime land-surface temperatures averaged between December 2016 and February 2017, showing visible light produced from anthropogenic sources (e.g. city lights) (Lee et al. 2006).

Figure 8. Top: Track of Typhoon Nida (source: Unisys Weather); Bottom: Rainfall total received from Typhoon Nida between August 1-5, 2016 (Rainfall product: the 3-hourly TMPA research product).

Figure 9. Time series from MERRA-2 showing seasonal and internal variations of monthly aerosol optical depth (top) and SO2 surface mass concentration (bottom) in PRD.

Figure 10. Similar to Fig. 9, except for CO surface concentration (top) and black carbon surface mass concentration (bottom).

Figure 11. Top: Time series of annual precipitation (in mm) in Maryland with hurricane contributed precipitation highlighted. Bottom: Average annual precipitation (in red) in Maryland

compared against annual precipitation with (in green) and without (in blue) hurricane contributed precipitation (units: mm).

Figure 1. Cities in Asia viewed from the 2016 annual NASA black marble, a nighttime view of the Earth, derived from a composite of data from the Visible Infrared Imaging Radiometer Suite (VIIRS) instrument on board the joint NASA/NOAA Suomi National Polar-orbiting Partnership (Suomi NPP) satellite (Lee et al. 2006). (Credit: NASA Worldview).

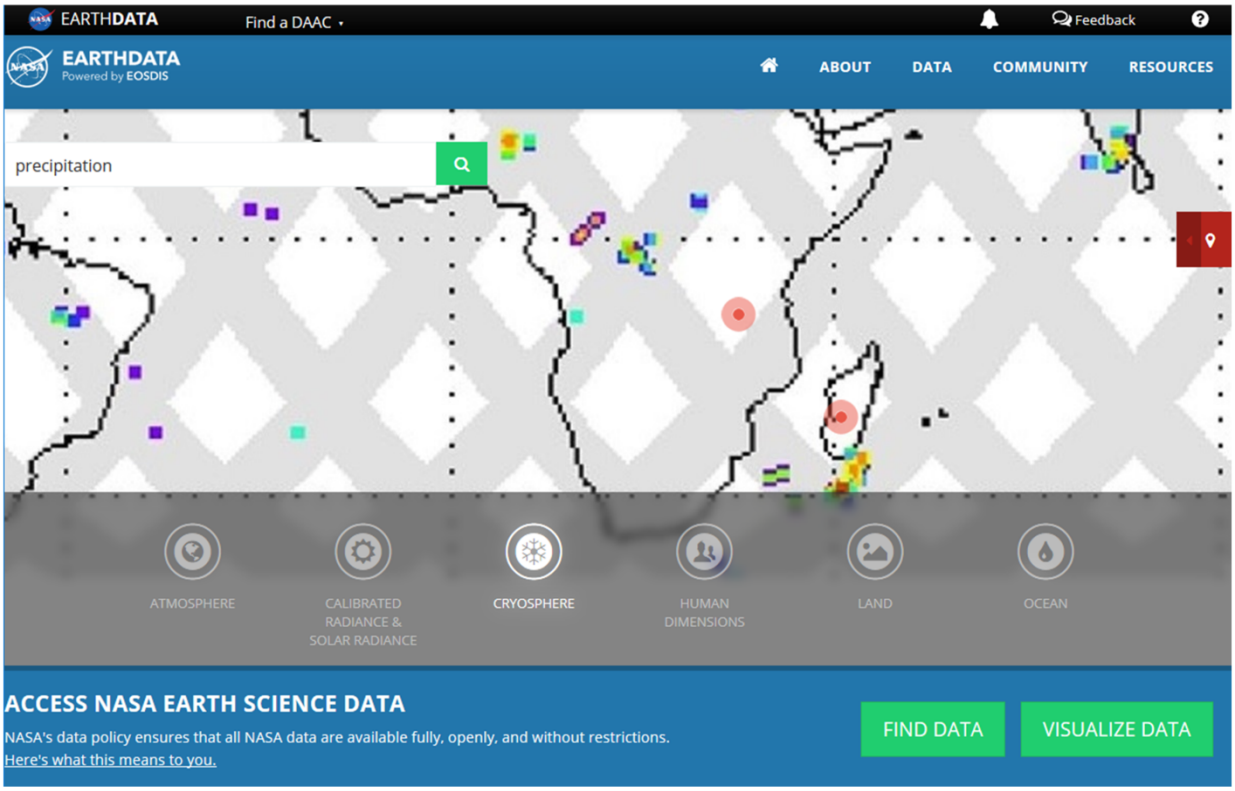

Figure 2. NASA Earthdata (NASA 2017b) provides a Web interface for searching and accessing NASA data at twelve EOSDIS DAACs.

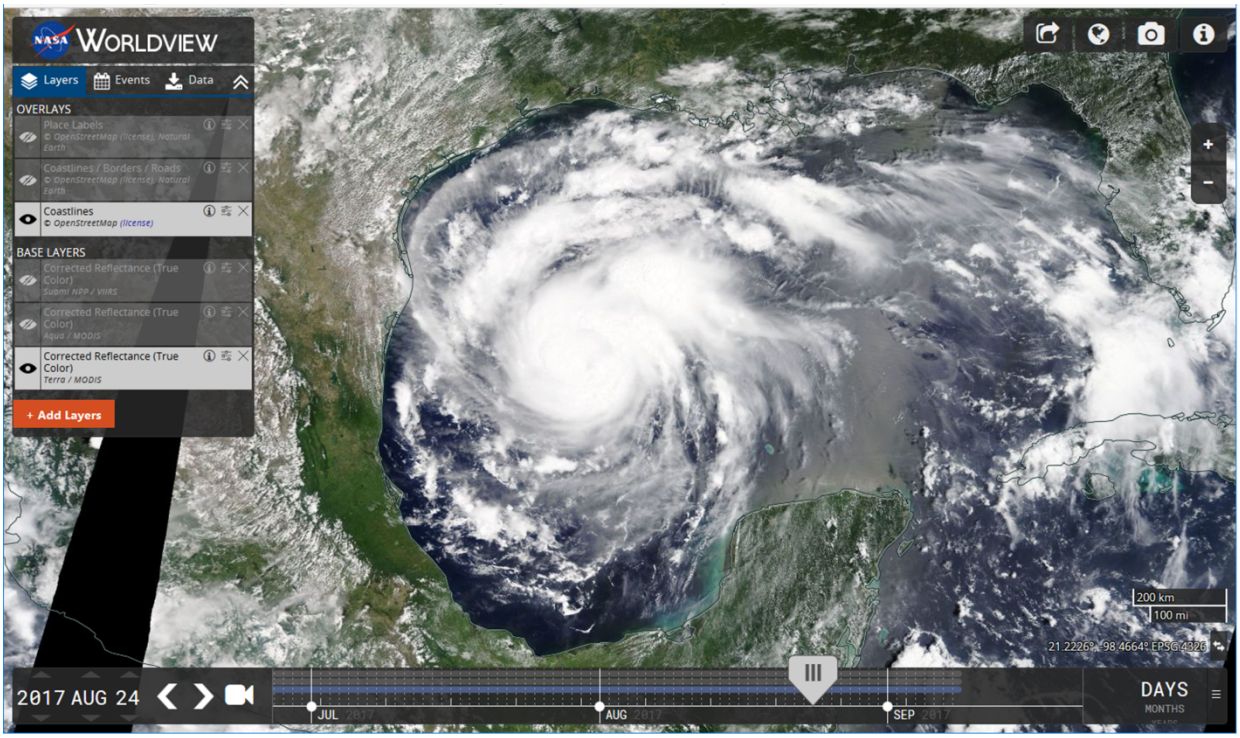

905

906 Figure 3. The NASA Worldview Web interface (NASA 2017g) showing Hurricane Harvey in
907 Gulf of Mexico on August 24, 2017.
908

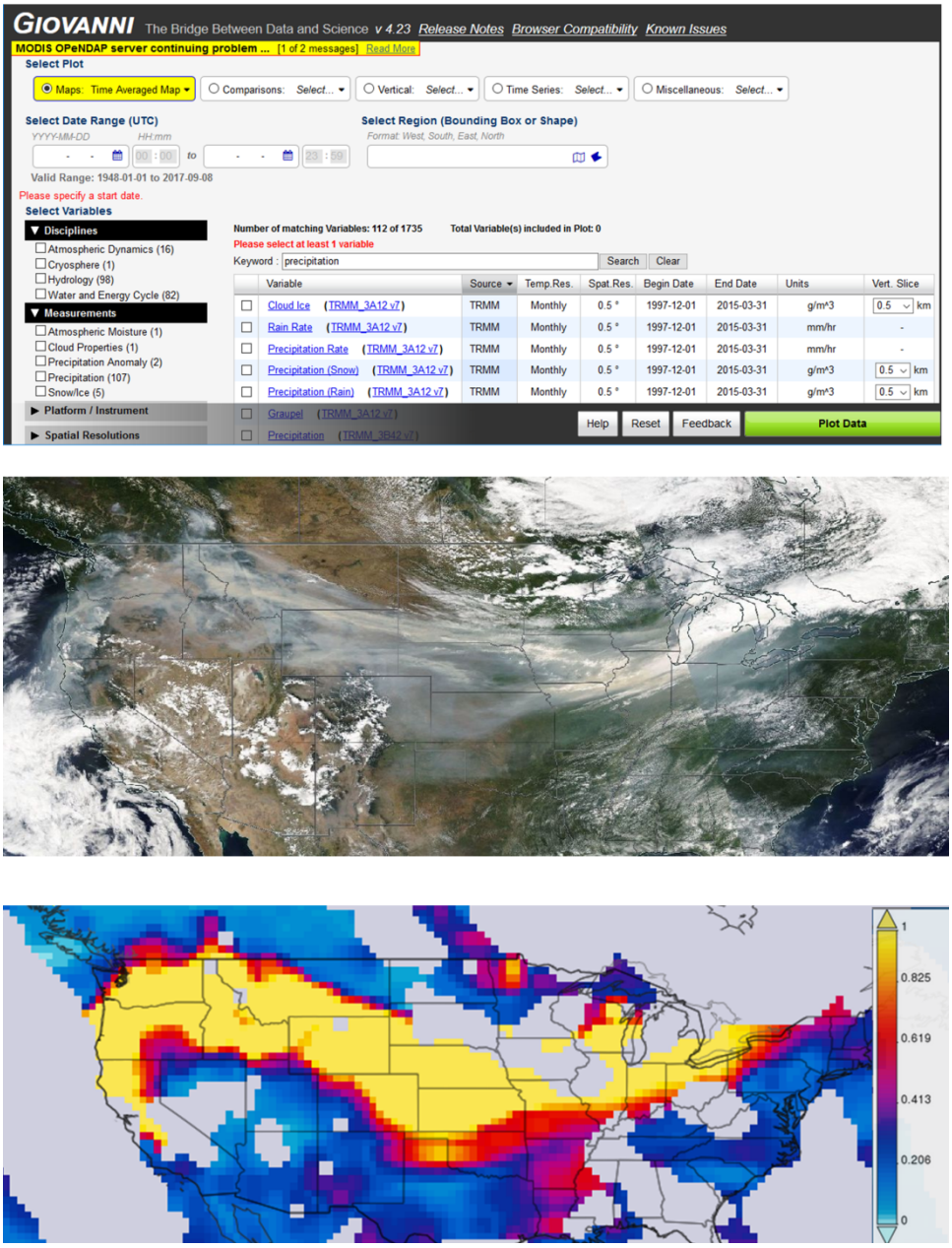

Figure 4. Top: The Web portal of NASA GES DISC Giovanni (NASA 2017h) with many features for easy locating a variable of interest, data analysis, and visualization; Middle: Corrected reflectance (true color) from MODIS Aqua on September 4, 2017, showing smoke from forest fires spreads across the United States and Canada (More detailed story is available at, https://earthobservatory.nasa.gov/IOTD/view.php?id=90899). Bottom: The combined dark target and deep blue aerosol optical depth (AOD) at 0.55 micron for land and ocean from MODIS Aqua on September 4, 2017. Combined with NASA Worldview, Giovanni provides analysis and visualization of the smoke aerosol for the event.

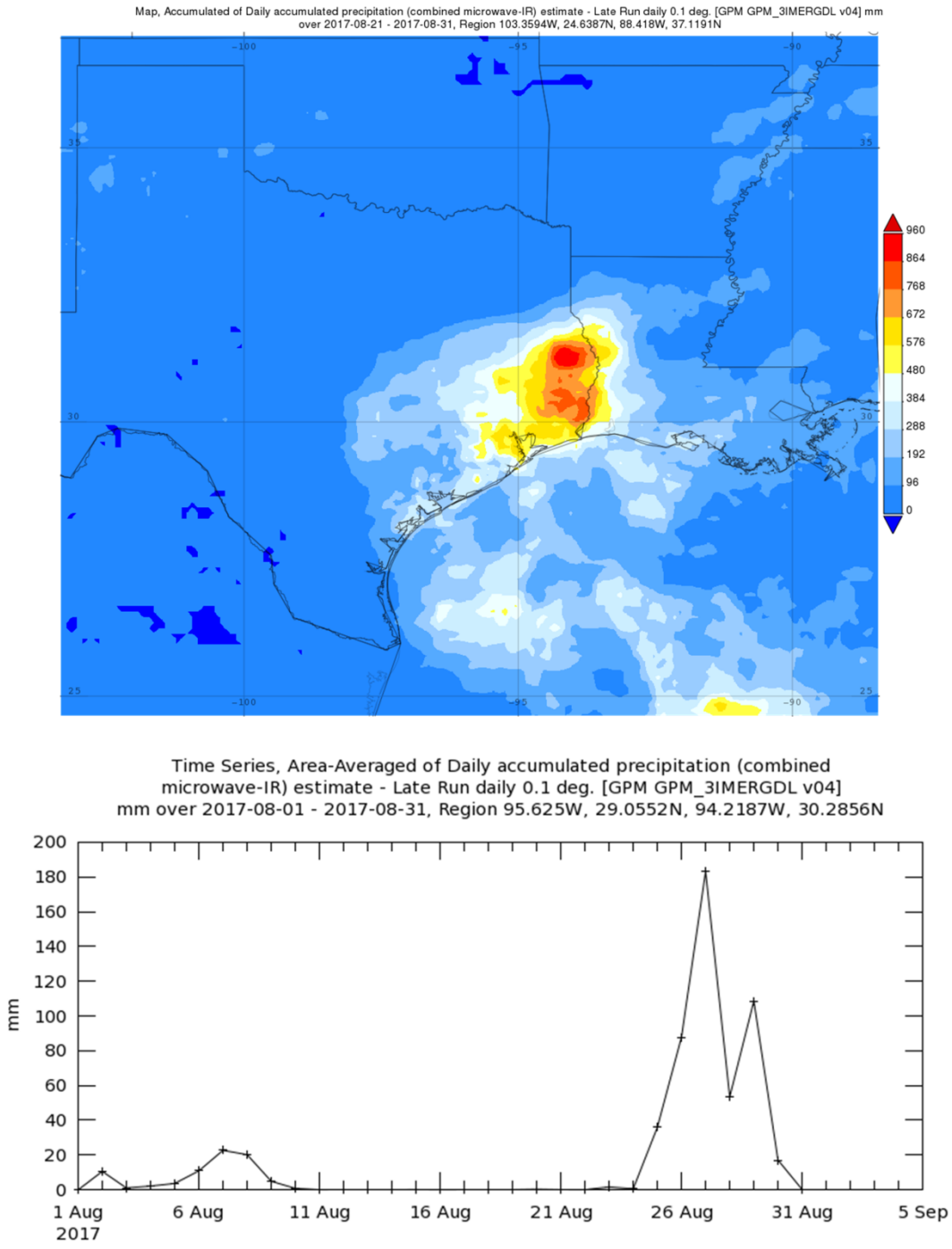

Figure 5. Sample graphics from Giovanni. Top: Accumulated rainfall (the GPM IMERG Late Run daily product) in mm from Hurricane Harvey (see Fig. 3) in Houston, Texas between August 21-31, 2017. Bottom: Time series of area averaged daily accumulated precipitation (mm/day) in Houston.

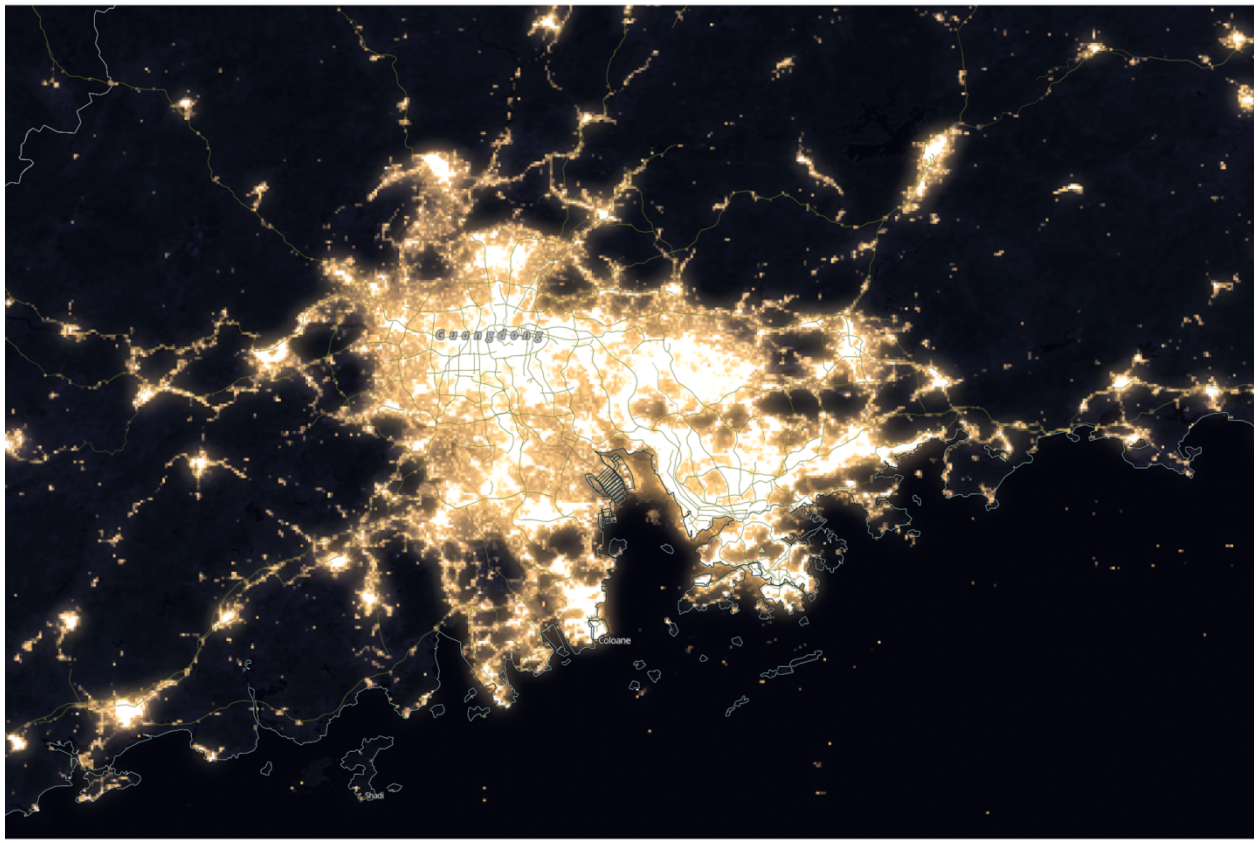

925

926 Figure 6. Similar to Fig. 1, except for the Pearl River Delta, showing visible light produced from
927 anthropogenic sources (e.g. city lights) (Lee et al. 2006).
928

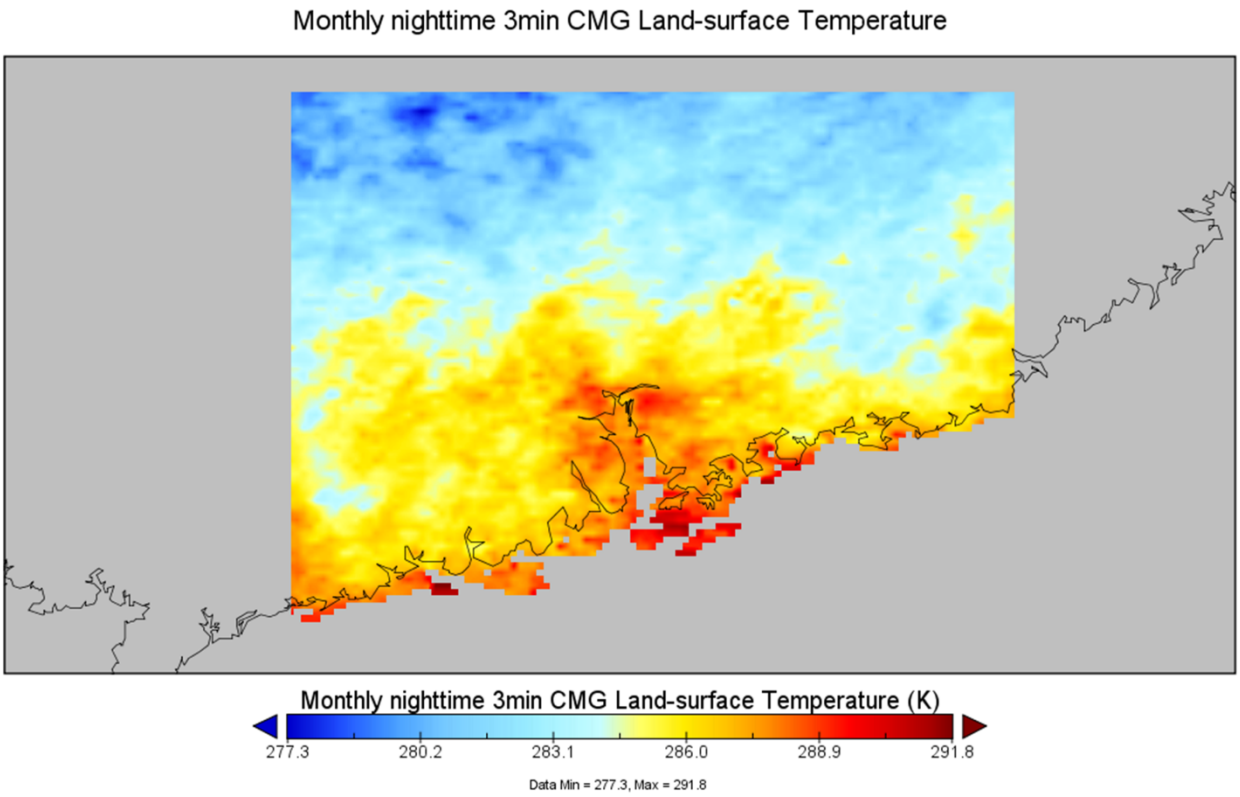

929

930 Figure 7. Map of MODIS-Terra monthly nighttime land-surface temperatures averaged between
931 December 2016 and February 2017.
932

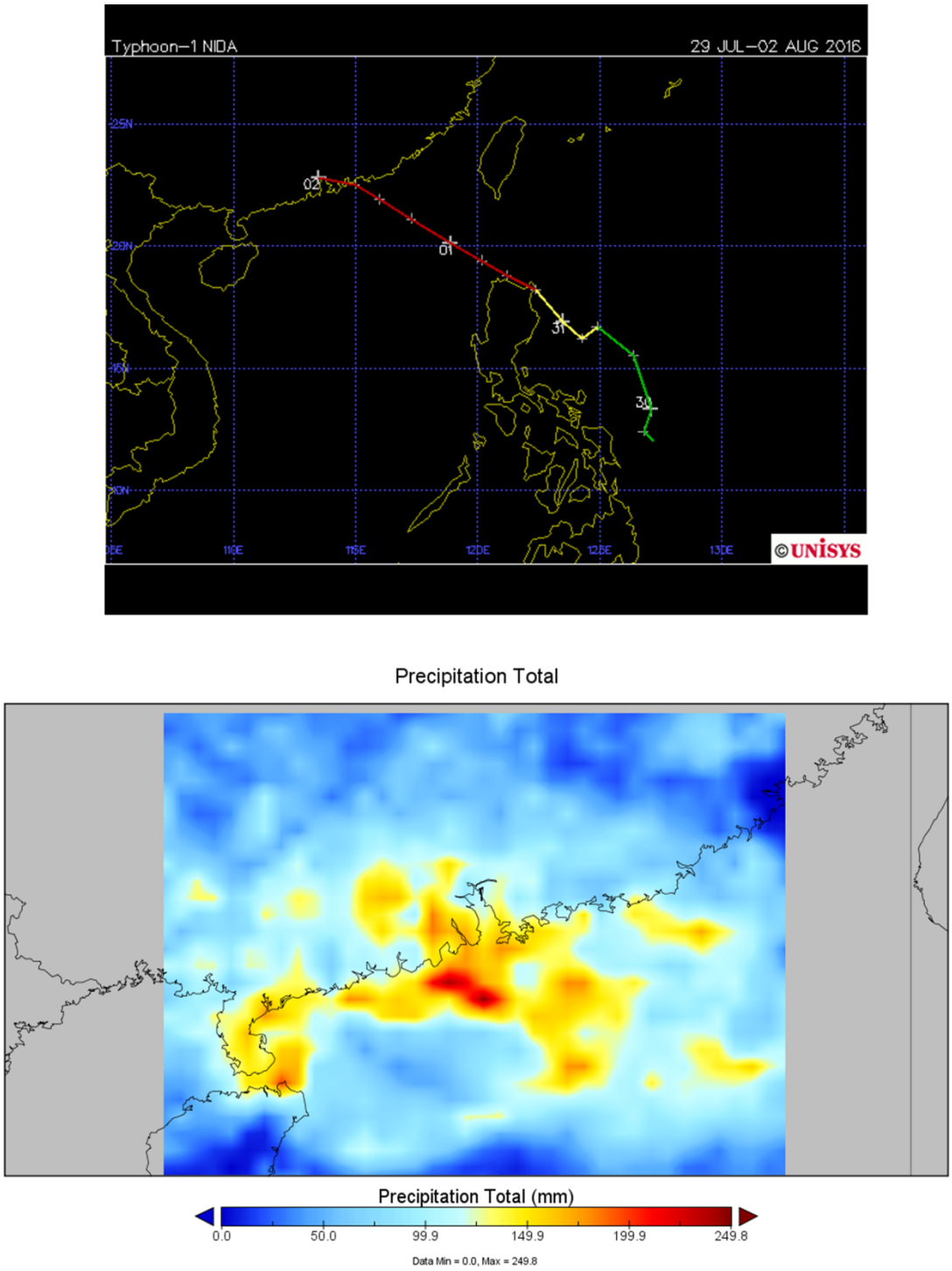

933

934 Figure 8. Top: Track of Typhoon Nida (source: Unisys Weather); Bottom: Rainfall total received
935 from Typhoon Nida between August 1-5, 2016 (Rainfall product: the 3-hourly TMPA research
936 product).
937

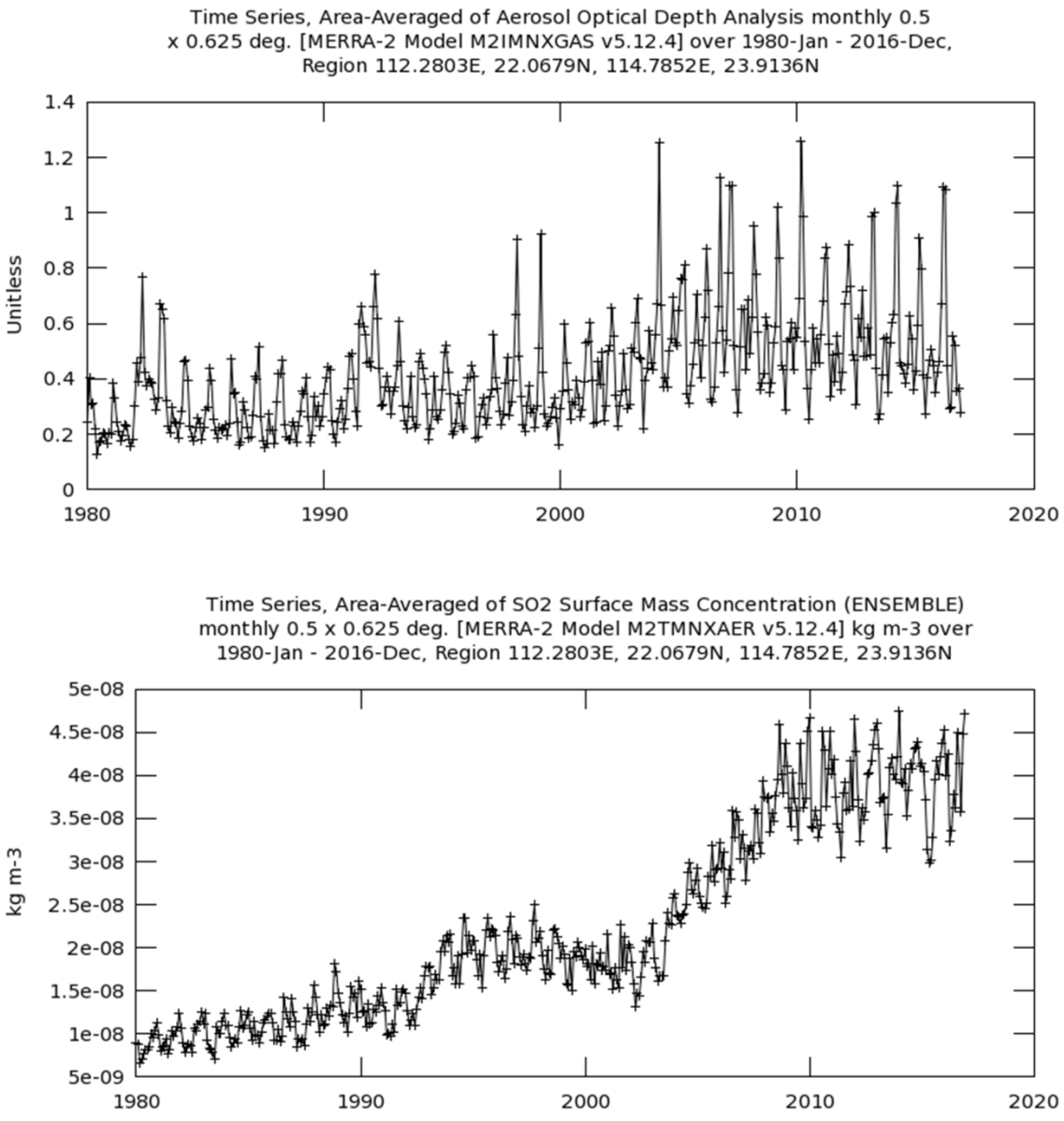

938

939 Figure 9. Time series from MERRA-2 showing seasonal and internal variations of monthly
940 aerosol optical depth (top) and SO2 surface mass concentration (bottom) in PRD.
941

942

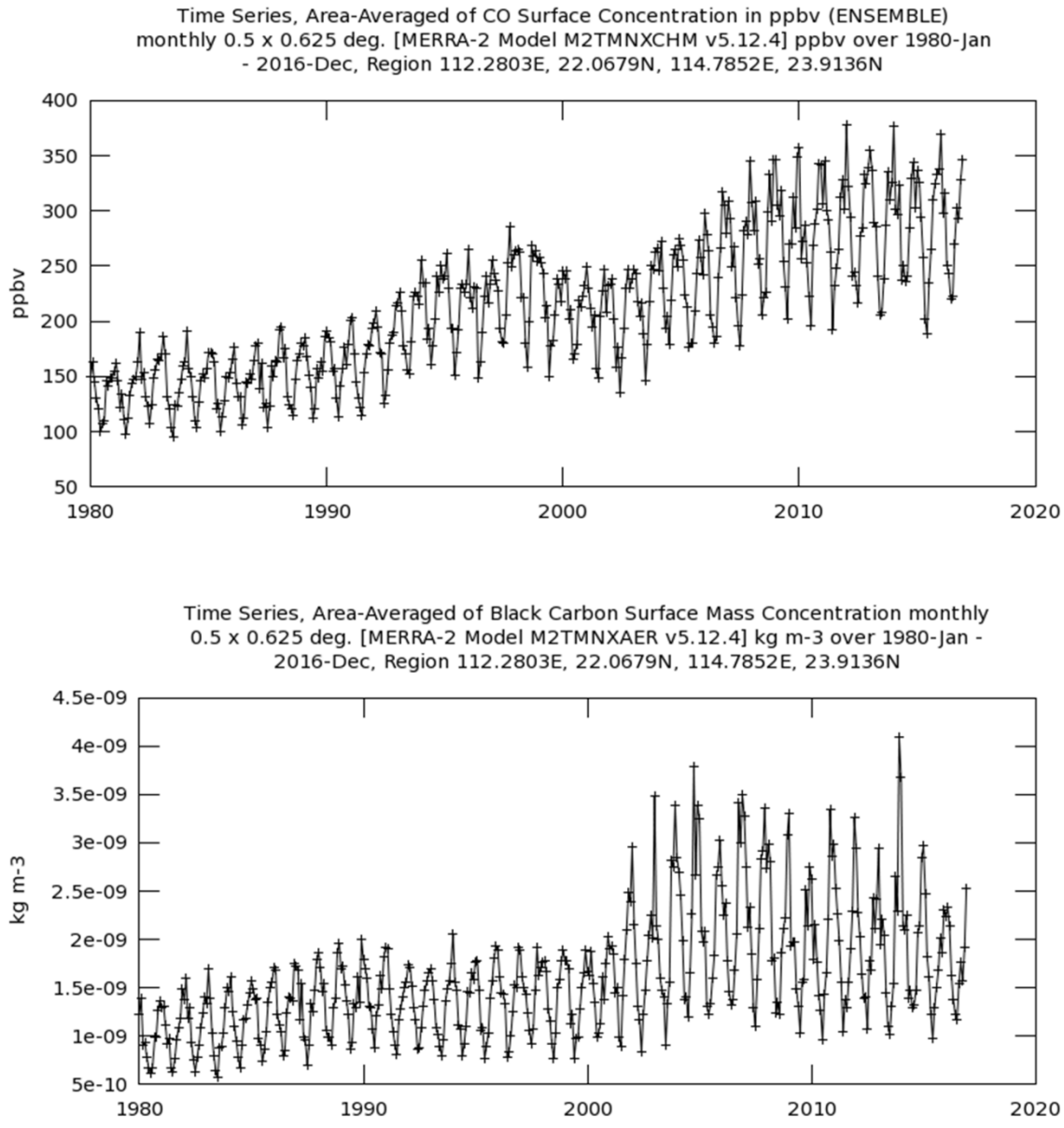

943

944 Figure 10. Similar to Fig. 9, except for monthly CO surface concentration (top) and black carbon
945 surface mass concentration (bottom).
946

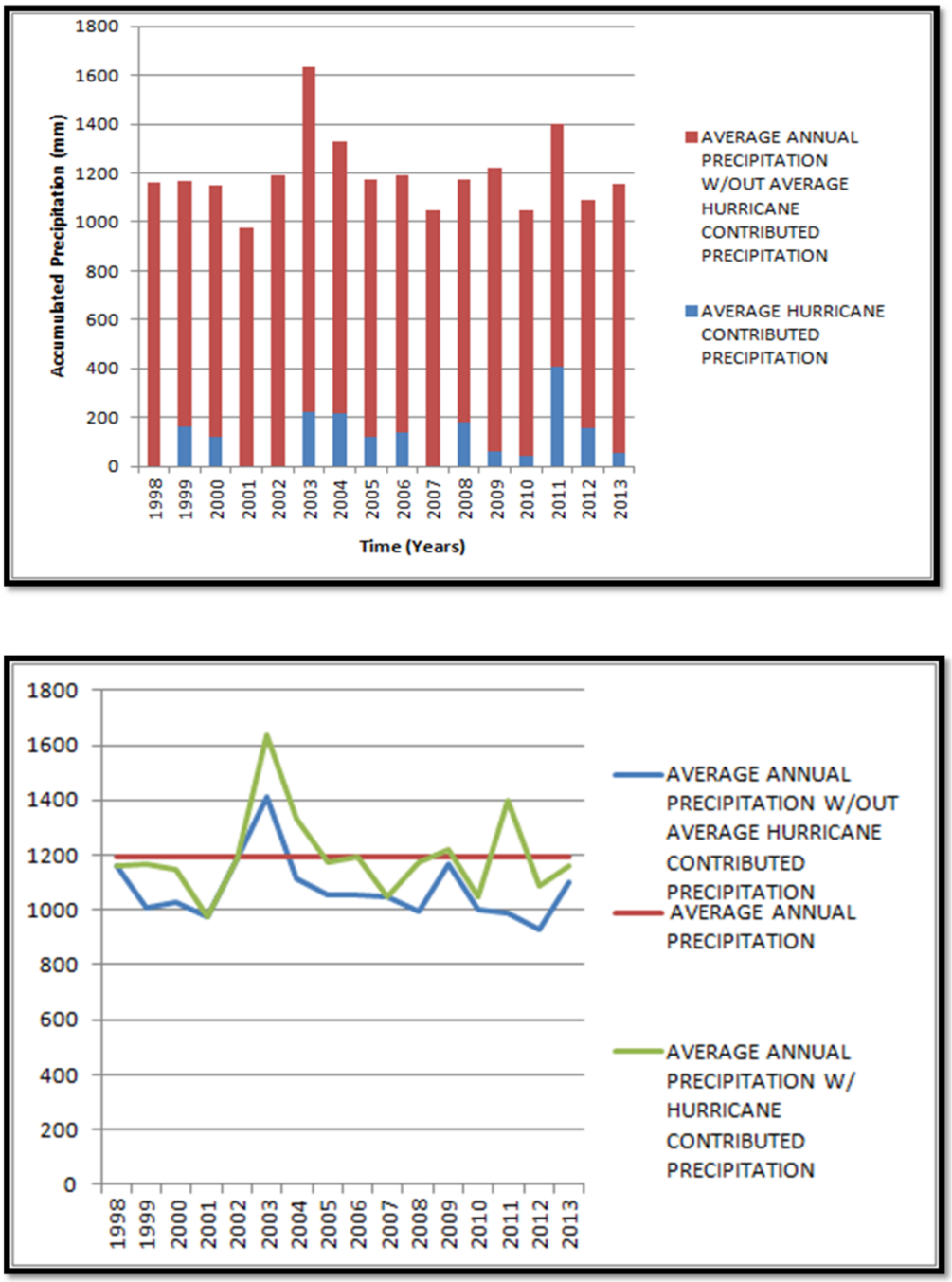

947

948 Figure 11. Top: Time series of annual precipitation (in mm) in Maryland with hurricane
949 contributed precipitation highlighted. Bottom: Average annual precipitation (in red) in Maryland
950 compared against annual precipitation with (in green) and without (in blue) hurricane contributed
951 precipitation (units: mm).